INTERFACES IN SOFT X-RAY MULTILAYER MIRRORS

Cover

The top image shows a cross-sectional transmission electron microscopy image of a failed W/Si multilayer deposition where the ion treatment of the W layers (dark) caused an increasing correlated roughness, resulting in a very high roughness of the top layer. The bottom image shows the result after optimization of the ion treatment.

Interfaces in soft x-ray multilayer mirrors
M.J.H. Kessels
Thesis, University of Twente, Enschede – Illustrated.
With references – With summary in Dutch and English
ISBN 90-365-2153-X

Press: Ponsen & Looijen, Wageningen

INTERFACES IN SOFT X-RAY MULTILAYER MIRRORS

PROEFSCHRIFT

ter verkrijging van
de graad van doctor aan de Universiteit Twente,
op gezag van de rector magnificus,
prof.dr. W.H.M. Zijm,
volgens besluit van het College voor Promoties
in het openbaar te verdedigen
op 10 maart 2005 om 13.15 uur

door

Marcus Jozef Henricus Kessels

geboren op 22 april 1977

te Roermond

Dit proefschrift is goedgekeurd door de promotoren:

prof. dr. K.J. Boller

prof. dr. A.W. Kleyn

en

assistent-promotor:

dr. F. Bijkerk.

The most exciting phrase to hear in science,
the one that heralds new discoveries,
is not 'Eureka!' (I found it!)
but 'That's funny ...'

Isaac Asimov
US science fiction novelist & scholar (1920 - 1992)

This thesis is based on the following publications:

Chapter 2: M.J.H. Kessels, J. Verhoeven, and F. Bijkerk, *Optimisation of reflectivity and selectivity of a multilayer mirror.* Submitted.

Chapter 3: M.J.H. Kessels, F.D. Tichelaar, J. Verhoeven, and F. Bijkerk, *determination of in-depth density profiles of multilayer structures.* Submitted.

Chapter 4: M.J.H. Kessels, J. Verhoeven, F.D. Tichelaar, and F. Bijkerk, *Ion induced interface layer formation in W/Si and WRe/Si multilayers.* Submitted.

Chapter 5: M.J.H. Kessels, J. Verhoeven, A.E. Yakshin, F.D. Tichelaar, and F. Bijkerk, *Ion beam induced intermixing of interface structures in W/Si multilayers.* Nuclear Instruments & Methods in Physics Research Section B- Beam Interactions with Materials and Atoms, 2004. **222** (3-4): p. 484-490.

Chapter 6: M.J.H. Kessels, J. Verhoeven, F.D. Tichelaar, F. Bijkerk, *Increased contrast and reduced intermixing in W/Si multilayer mirrors by H-passivation.* In preparation.

The author was also co-author of the following publications and patents:

E. Louis, A.E. Yakshin, P.C. Görts, S. Oestreich, R. Stuik, M.J.H. Kessels, E.L.G. Maas, F. Bijkerk, M. Haidl, S. Müllender, M. Mertin, D. Schmitz, F. Scholze, and G. Ulm. *Progress in Mo/Si multilayer coating technology for EUVL optics*. in *Emerging Lithographic Technologies IV, SPIE's 25th Annual International Symposium on Microlithography*. 2000. Santa Clara: SPIE.

E. Louis, A.E. Yakshin, P.C. Görts, S. Oestreich, E.L.G. Maas, M.J.H. Kessels, D. Schmitz, F. Scholze, G. Ulm, S. Müllender, M. Haidl, and F. Bijkerk. *Mo/Si multilayer coating technology for EUVL, coating uniformity and time stability*. in *SPIE's 45th Annual Meeting*. 2000. San Diego: SPIE.

E. Louis, A.E. Yakshin, S. Oestreich, P.C. Görts, M.J.H. Kessels, E.L.G. Maas, F. Bijkerk, S. Müllender, M. Haidl, J. Tümmler, F. Scholze, and G. Ulm. *E-beam coating technology for EUVL optics*. in *Second SEMATECH Workshop on Extreme UV Lithography*. 2000. San Francisco: International Sematech.

F. Bijkerk, E. Louis, M.J.H. den Hartog, M.J.H. Kessels, and J. Verhoeven, *Meerlagenspiegel voor straling in het XUV golflengtegebied en werkwijze voor de vervaardiging daarvan*, patent number NL1018139, priority date 23 May 2001.

F. Bijkerk, A.E. Yakshin, E. Louis, M.J.H. Kessels, E.L.G. Maas, and C. Bruineman, *Method for coating substrates and mask holder*, patent number US2004/0052942 A1, priority date 18 March 2004.

S. Dobrovolskiy, A.E. Yakshin, M.J.H. Kessels and J. Verhoeven, *The application of energetic CH_x^+ ions to form a Si/SiC multilayer systems for reflection of radiation between 20 and 80 nm,* Submitted.

PHILIPS

This work is part of the research of the Stichting voor Fundamenteel Onderzoek der Materie (FOM), financially supported by the Nederlandse Organisatie voor Wetenschappelijk Onderzoek (NWO), and Philips Research. The patent *Method for coating substrates and mask holder* has been financed by Carl Zeiss AG.

Table of Contents

1 Introduction

1.1 Motivation

Our visual perception consists of the ability to detect electromagnetic radiation and to interpret it. Unfortunately, our eyes can only detect a limited range of the electromagnetic spectrum, namely the visible light. This prevents us for example to see heat (which is in the infra-red spectrum) or to see through tissue (which requires x-ray vision). An additional advantage of x-ray vision would be the ability to detect much smaller details, since the smallest features visible are generally as large as the wavelength of the light employed for their imaging. The potential of x-ray vision is to see details smaller than 20 nanometer, a factor of ten below the visible light limit. To make such details visible to the human eye, one needs a device to magnify them using x-ray radiation, and to convert the x-ray image into a visible image: one would need an x-ray microscope.

X-rays do not just allow the observation of such small objects, they also allow one to *create* images at a nanometer scale, basically by using the microscope in the reverse optical direction. This feature is of special interest to the semiconductor industry for the fabrication of transistors in next generation lithography processes. According to Moore's law, the number of transistors within a computer chip is being doubled every 18 months. This necessitates a continuous reduction of the size of these transistors. Currently, the semi-conductor industry is about to demonstrate the first machine to produce computer chips using x-ray radiation (13.5 nm), for this particular application named Extreme UltraViolet (EUV).
Another application of x-rays is found in the field of X-Ray Fluorescence spectrometry (XRF). XRF is applied to measure the element specific fluorescence radiation of samples

after excitation by high-energy photons. This technique enables the quantitative determination of the elemental composition of the sample.

In all these applications the availability of x-ray optical elements are mandatory. However, due to the high absorption and low refractive index of materials in this wavelength range, neither lenses, nor classical (single reflection) mirrors can be applied. Fortunately, using positive interference of reflected waves, it is still possible to achieve an acceptable reflectivity. A multilayer mirror is based on this, well-known, principle, which is shown in Figure 1. At each transition from one material to another partial reflection occurs. By carefully selecting the thicknesses of these layers, positive interference occurs, and all individual reflections add up. In section 1.3 the multilayer mirror principle is explained in more detail.

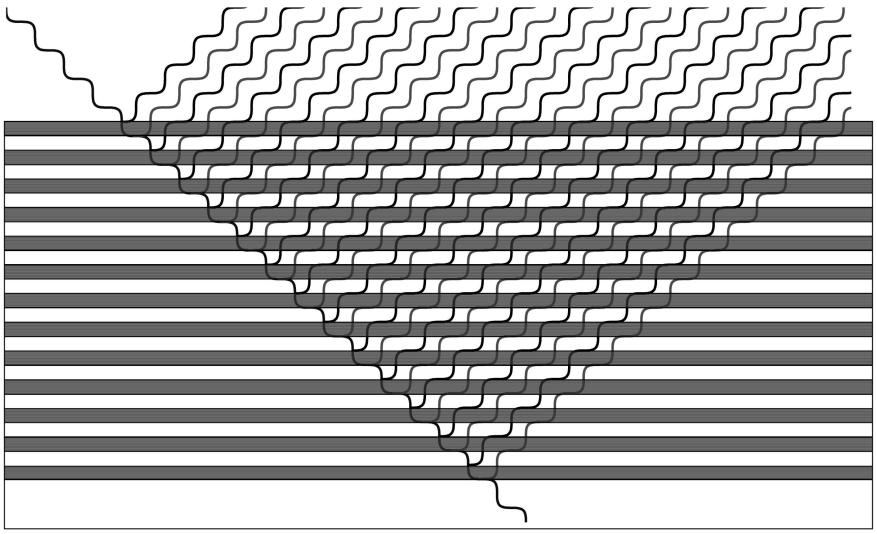

Figure 1 Principle of a multilayer mirror

Methods to improve these mirrors have been studied since 1912, the year in which William Henry Bragg and William Lawrence Bragg formulated, what is now called, the Bragg equation: $n\lambda = 2d \sin \alpha_i$, i.e. the basic relation between the incident wavelength, λ, the multilayer periodicity, d, and the grazing angle of incidence, α_i. This also reveals that such a multilayer mirror is a wavelength dispersive element, i.e. it reflects a certain wavelength only at a specific angle, an important advantageous property for the XRF application.

More than 90 years after the first understanding of the Bragg reflection, x-ray optics research, including multilayer optics,[1] is more alive then ever. The challenges of realizing 'x-ray vision' in a number of major applications provide an enormous motivation for basic research activities. This thesis addresses solutions to a number of so far unsolved research issues which are essential for a range of applications. A first issue deals with multilayer design and the choice of the wavelength selectivity. In the past it has both experimentally[2,3] and theoretically[4] been demonstrated that it is possible to increase the multilayer selectivity by adjusting the optical refractive indices within each period. However, until now it was unknown what profile would result in the highest reflectivity at a pre-set selectivity. Filling this void, a theoretical demonstration of the most optimal profiles is given, which turned out to be, in contrast to earlier suggestions, profiles with sharp interfaces (chapter 2). The selectivity could be adjusted by selecting a different thickness ratio between the two materials.

A second issue addressed deals with the multilayer reflectivity. The research for the highest reflectivity was accelerated from 1992 onward, when the semiconductor industry put EUV on their technology road map. This effort resulted in a world record of 69.5% reflectivity on a standard Mo/Si multilayer mirror, deposited in our group.[5] The record for non-standard multilayer mirrors is currently 69.8%, measured on a Mo/B_4C/Si/C multilayer.[6] Although these values are already very close to the theoretical maximum for standard Mo/Si systems (74%), the EUV Lithography (EUVL) application still demands higher reflectivities.

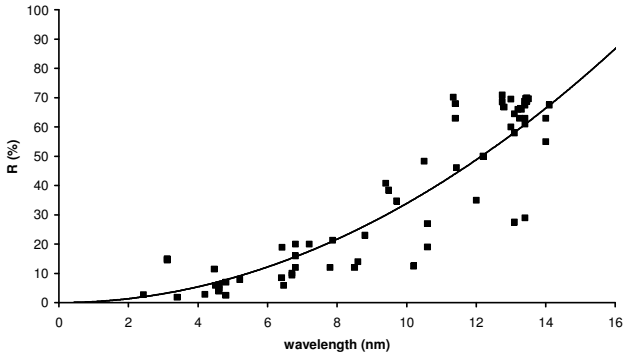

Figure 2 Demonstrated near normal incidence reflectivities as a function of wavelength as reported at the Physics of X-ray Multilayer Structures (PXRMS) conferences. The quadratic wavelength dependence is indicated.

In general, at shorter wavelengths lower reflectivities are achieved. Figure 2 shows the peak reflectivity as a function of the wavelength, as presented by a large number of researchers at the different conferences on the Physics of X-Ray Multilayer Structures (PXRMS).[7] The lowing of the reflectivity toward shorter wavelengths is mainly due to physical properties of the materials at these wavelengths: the refractive index contrast between the two materials decreases with wavelength, being roughly proportional to the square of the wavelength. This basically limits the reflectivity, as well as the choice of practically suitable materials. Additionally, the widths of the interfaces between the materials become more important when the thickness of the layers is reduced, causing a relatively larger spread of the phase distribution of the reflected radiation. Both points mentioned, - the desired degree of perfection for the relatively long-wavelength EUVL application and - the inherent difficulty of producing thin interlayers in short-wavelength multilayer applications, urge for a continued effort on optimizing the fundamental growth processes of multilayer structures. Ion beam smoothening was applied during or after layer deposition, a powerful method, still not fully exploited in research. It is especially appropriate for the above cases due to the ability to apply it very locally, i.e. to thin slices of the multilayer stack (chapter 4 and 5).[8]
In chapter 6 another method to change the interface width is introduced. In contrast to the ion beam smoothening, which in principle is a mechanical treatment, the chemical properties of the material at the interfaces were modified. Using this method an origin of the natural interlayer formation, namely diffusion, is prevented.

To be able to apply such ion treatments successfully, it is imperative to avail oneself of non-destructive analysis techniques with sufficient depth resolution. This leads us to the third issue addressed in this thesis: the development of such analysis method, since most existing methods have inherent limitations for our goal. For instance, the most obvious, and straightforward method, the measurement of the angle dependent reflectivity, only yields a measure of the overall performance of the structure, without useful information on the structure itself. The reason for this, the lack of phase information from reflectivity measurements, leads to non-unique solutions for the structure, the so-called inversion problem. Numerous methods have been published to overcome this problem, some using extensive assumptions of the expected structure,[9] on the expected phase information[10] or a combination of both.[11] All methods thus depend on a-priori known data or fitting routines using a large number of free parameters.
Additional techniques, based on the interaction with photons, ions or electrons can be employed. The most common methods are listed in Table 1. The majority of these are

Technique	Basic principle	Advantages	disadvantages
XPS	photons excite atoms, which emit an inner-shell electron	non-destructive, elemental specific	no in-depth information
XRF	photons excite atoms, which emit an x-ray photon	non-destructive, elemental specific	no in-depth information
(L/M/H)EIS and RBS	energetic ions scatter at structure, structure can be determined from energy loss	in principle elemental specific	may destroy structure during measurement
SIMS	ions sputter and ionize material from surface, with mass measured using mass spectrometers	high material selectivity	no in-depth information, limited lateral resolution
TEM	transmitted energetic electrons are imaged	high in-depth resolution, relatively non-destructive	no calibration of intensity scale
EELS	measurement of loss of energy of transmitted electrons	non-destructive, elemental specific	resolution is less than TEM
HAADF	measures diffraction angle of forward scattered electrons	non-destructive, quantitative elemental analysis	limited to high Z materials
AES	electrons excite atoms, which emit an electron	sensitive for chemical compositions	limited lateral resolution, only surface
EDX	electrons excite atoms, which emit a photon	high material selectivity	limited lateral resolution, averages over large depth scale
SEM	electrons excite atoms, emitted electrons are imaged	works well with 3D structures	limited lateral resolution, averages over large depth scale
AFM	scans surface with needle, measures forces	very high lateral resolution	material-independent, no in-depth information
STM	scans surface with needle measuring tunnel current	very high lateral resolution, can distinguish materials	no in-depth information, needs conducting surface

Table 1 overview of analysis techniques available for multilayer structure determination.

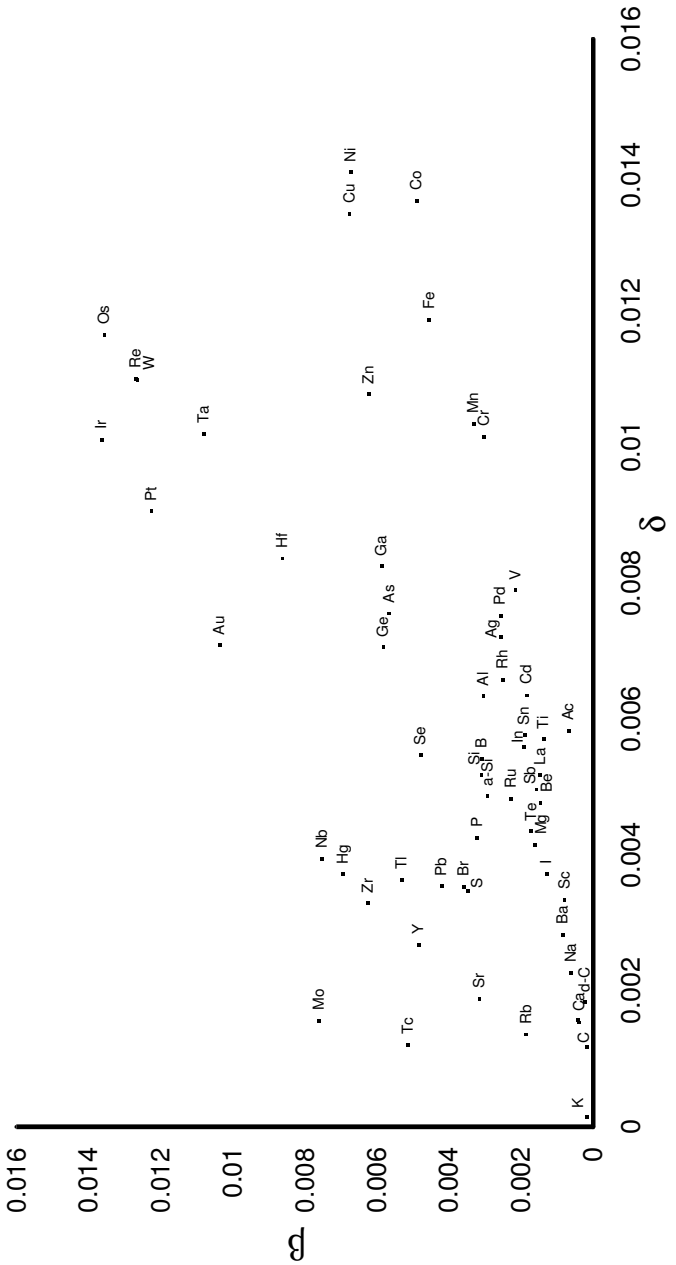

Figure 3 Refractive indices $\boldsymbol{n} = 1-\delta-i\,\beta$ of the elements at a wavelength of 4.46 nm.

surface techniques, and hence require a method to sample thin slices of the structure by depth profiling, obviously illustrating their destructive character.
In chapter 3 a method is introduced that does not alter the structure of the sample prior to or during the analysis, and that does not require a priori knowledge of the structure. The method is based on cross section TEM, calibrated by CuKα reflectometry data. This allows a quantitative in-depth density profile, which is not based on a-priori known information of the structure.* This new technique made it possible to analyze the influence of the ion beam smoothening procedure on the individual interfaces within the multilayer structure.

Having thus introduced the three main topics addressed in this thesis, - design, - growth, and - analysis of multilayer interfacial structures, I now proceed to summarize the theory of x-rays optics and the experimental setup used to investigate and create the multilayer mirrors.

1.2 X-ray optics

1.2.1 Basic principles

By definition, x-rays are a form of electromagnetic radiation produced following the ejection of an inner orbital electron and subsequent transition of atomic orbital electrons from states of high to low energy.[12] According to this definition, the wavelength of x-ray radiation ranges from 0.01 to ~23 nm. X-rays with a wavelength longer than 0.1 nm are called soft x-rays. At wavelengths shorter than this, they are called hard x-rays. Hard x-rays overlap the range of gamma rays, which are generated by transitions within atomic nuclei. At the long wavelength side x-rays are adjacent to EXtreme UltraViolet (E/XUV) radiation. Also on this side an overlap between two regions exists, although this overlap is not based on any physical arguments: wavelengths longer than 10 nm are usually referred to as XUV. Notably the term EUV, mostly used to indicate the wavelength of 13.5 nm, has been proposed for EUV lithography.

* In cross section TEM the sample is cut into a slice of approximately 1 mm wide. Using mechanical grinding and ion beam milling this is further reduced down to 100 nm. Although the edges (~5 nm) are altered by this milling, the bulk of the cross-sectional structure is measured in its original state, so that TEM images represent the true in-depth structure.

1.2.2 Refractive optics

Unlike visible light, x-rays hardly refract or reflect, due to the fact that the refractive index $\boldsymbol{n} = 1-\delta-i\beta$ is close to 1, as can be seen from Figure 3 where the real (δ) and imaginary (β) part of the refractive index are visualized for the elements at a wavelength of 4.46 nm. Because of this close-to-unity value of $\boldsymbol{n}$, lenses should be very thick to create any noticeable refraction. However, all radiation will be absorbed in that case due to the relatively large absorption in the soft x-ray region (complex part of the refractive index).

1.2.3 Diffractive optics

Geometrically similar to lenses are Fresnel zone plates. Unlike lenses, zone plates make use of diffraction. Diffraction is the bending of light when it skims the edges of an opaque object. Zone plates consist of a central opaque zone surrounded by alternating transparent and opaque zones of increasing radius and decreasing width. The radii of the zone plate edges are given by:

$$r_n^2 = nf\lambda + \frac{1}{4}n^2\lambda^2 \quad , \qquad (1)$$

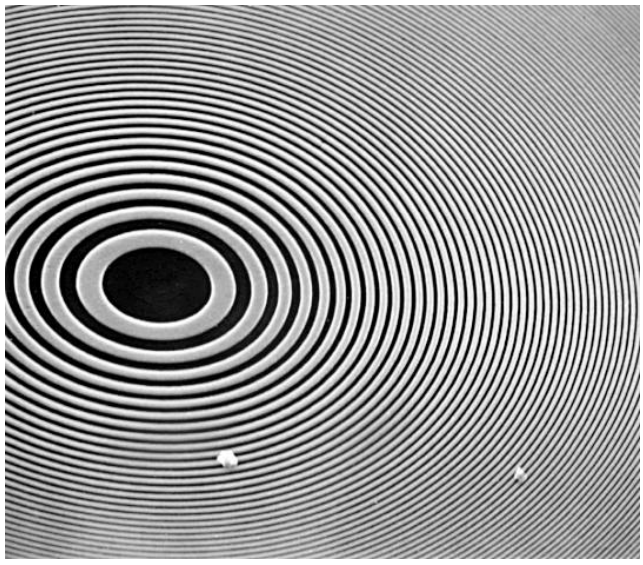

Figure 4 Scanning electron microscope image of the inner part of a Fresnel Zone Plate Lens. This lens has 318 nickel zones, a diameter of 45 µm, and the smallest (outermost) zone is 35 nm wide. Image obtained from http://www-cxro.lbl.gov/microscopy/zp.gif

where n is the zone number (opaque and transparent zones counted separately) and f is the first order focal length.

In theory, the maximal efficiency to of such a zone plate to focus radiation in the first order is π^{-2} (~10%). This is because most of the radiation is absorbed by the opaque zones (50%) and the remaining radiation is diffracted in other orders (zeroth order 25%, negative orders 12.5%, and higher positive orders 2.5%). Twice the efficiency can be obtained when the opaque zones are replaced by transparent, phase shifting zones.[13] The finest spatial resolution of an image produced with a Fresnel zone plate is governed by the Rayleigh criterion, resulting in a value for the resolution of 1.22 Δr, where Δr is equal to the width of the outermost zone. Using advanced e-beam pattern writing it is possible to make zone plates having a Δr as small as 35 nm, as is shown in Figure 4. However, the size of this zone plate scales also with the width of the outer zone:

$$D = 4N\Delta r \qquad (2)$$

where N equals to the number of zones. To avoid chromatic blurring this number should be limited to:

$$N < \frac{\lambda}{\Delta\lambda} \quad , \qquad (3)$$

where $\Delta\lambda$ equals to the spectral width of the illuminating radiation. This commonly results in zone plates with a size of 50 μm when applied for soft x-ray radiation. Thus, to collect as much radiation as possible from a point source, the zone plate should be located very close to the source. Because most laboratory soft x-ray sources, like laser produced plasma's and discharge produced plasma's are based on hot, expanding plasmas, they impose limitations on the collecting optics, making the delicate zone plates unsuitable as a collecting optical element.

1.2.4 Reflective optics

As an alternative to the light transmitting optics described above, it is also possible to manipulate radiation by reflection. According to the Fresnel equations:[14]

$$r_s = \frac{\sin\alpha_1 - \sqrt{n^2 - \cos^2\alpha_1}}{\sin\alpha_1 + \sqrt{n^2 - \cos^2\alpha_1}} \text{ and} \qquad (4a)$$

$$r_p = \frac{n\sin\alpha_1 - \sqrt{n^2 - \cos^2\alpha_1}}{n\sin\alpha_1 + \sqrt{n^2 - \cos^2\alpha_1}}, \qquad (4b)$$

the reflected amplitudes r_s and r_p for s and p polarization respectively, depend on the grazing angle of incidence α_1 and the relative complex reflective indices $\boldsymbol{n}= \boldsymbol{n}_2/\boldsymbol{n}_1$, which equals to the fraction of the refractive indices of the refracting ($\boldsymbol{n}_2$) and incident ($\boldsymbol{n}_1$) media. The reflectivity is then calculated using:

$$R = rr^*, \qquad (5)$$

where r^* is the complex conjugate of r. In Figure 5 the calculated reflectivity of a tungsten mirror for s- and p-polarized radiation with a wavelength of 4.4 nm is shown. From this graph it becomes clear that the reflected intensity at all but very grazing angles is low. The major part of the radiation is absorbed in the W mirror. The transmitted amplitude can be calculated using similar formulas as for the reflected amplitude, but also more directly using:

$$t_s = r_s + 1 \ , \qquad (6a)$$

$$t_p = \frac{\left(r_p + 1\right)}{\boldsymbol{n}} \ . \qquad (6b)$$

However, due to the high absorption of soft x-rays, 97% of the radiation will be absorbed within typically 100 nm.

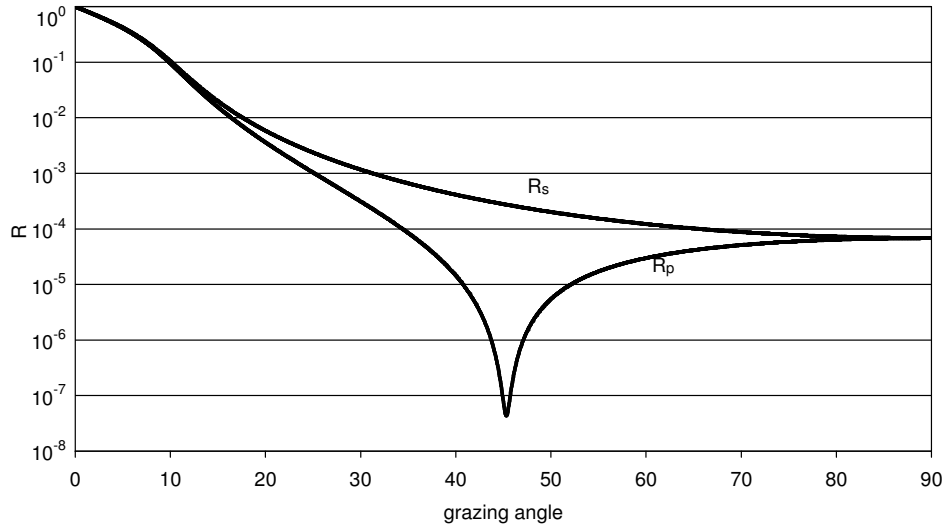

Figure 5 Calculated reflectivity of s and p polarised radiation with a wavelength of 4.4 nm on a W mirror.

To increase the reflectivity beyond what is obtainable using a single surface, one could attempt to reflect the transmitted radiation again before it is absorbed in the structure. A multilayer mirror is based on this principle, and will be discussed in the next section in more detail.

1.3 Theory of multilayer mirrors

A multilayer mirror (Figure 1) is a stack of layers of (at least) two alternating materials of which one material has a low refractive index (high δ, dark layers) and the other material has a high refractive index (low δ, white layers). From this figure the basic principles are evident: at each interface between the two materials a (small) part of the incoming radiation is reflected and the remaining part is transmitted. At the first interface (vacuum/ high δ) *internal* reflection occurs. This is due to the fact that the refractive indices for x-rays of nearly all materials are below one, which is in contrast to the indices for visual light. At the next interface (high δ / low δ) *external* reflection occurs. This also adds an additional phase shift of 180º to the reflected radiation. By carefully selecting the layer thicknesses, all reflected radiation will add up in phase. This is accomplished when the thickness d of each period (the combination of two layers) satisfies the Bragg equation:

$$n\lambda = 2d \sin\alpha_i , \qquad (7)$$

where n is an integer number representing the Bragg order.
The thickness of the individual layers should, when not taking into account absorption, be equal to half of the period thickness. Taking absorption into account, the reflectivity of the structure can be increased by reducing the thickness of the most absorbing material (high β), while keeping the period thickness constant.
From the Bragg equation it is also evident that a multilayer mirror is a dispersive element: each wavelength is only reflected at one particular angle, for each Bragg order. However, this assumes an infinite number of periods, which is practically not feasible. As a consequence of the limited number of periods, a specific wavelength is reflected at a small angular range $\Delta\theta$. Therefore each mirror can be characterized using its reflectivity R and its angular selectivity $\theta/\Delta\theta$. As an alternative, one might also select a fixed angle, and look at the wavelength range $\Delta\lambda$ reflected at this angle. This can then be expressed as a wavelength selectivity $\lambda/\Delta\lambda$.

1.3.1 Fourier method

The reflectivity and selectivity of a multilayer structure can be calculated using several theoretical models. The Fourier method[10] allows an analytical solution, based on the

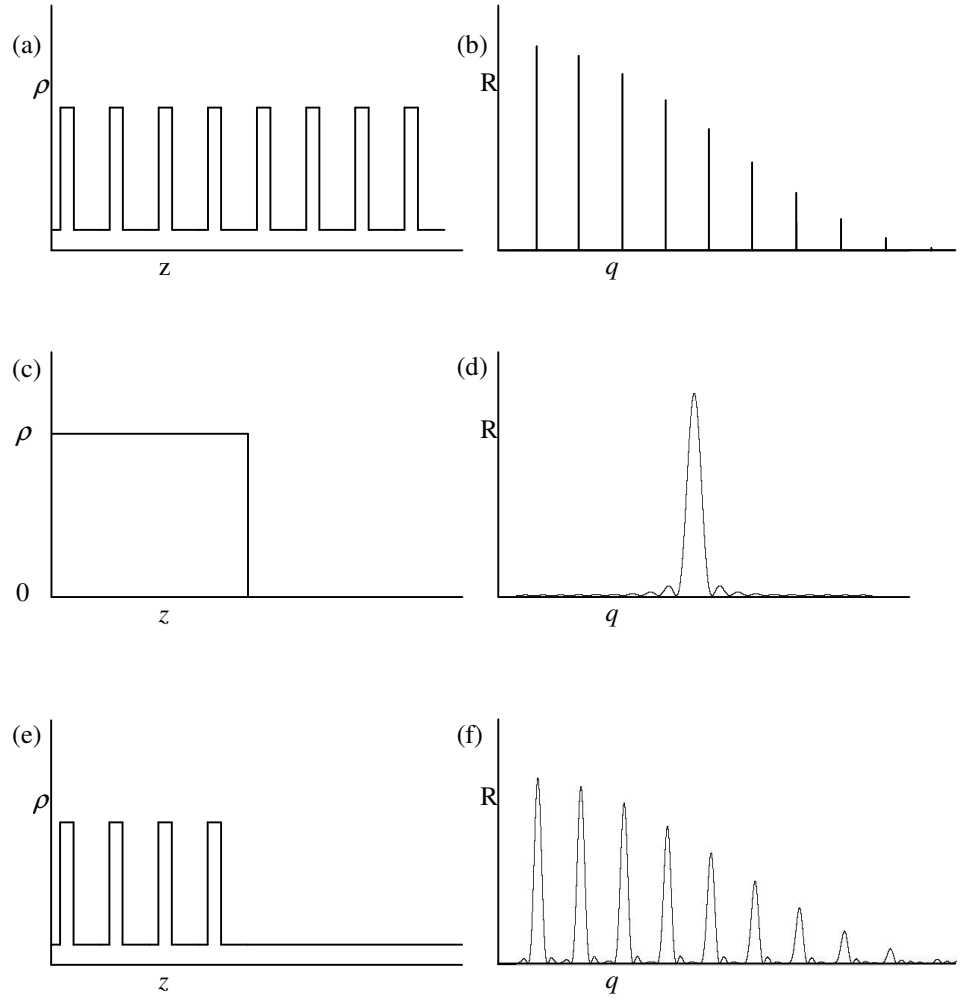

Figure 6 Explanation of influence of limited number of periods on selectivity. Electron density profile of a semi-infinite stack (a) and its reflectivity spectrum as calculated with the Fourier method (b). The envelope function used to limit the number of periods (c) and its Fourier transformation (d). The final density profile (e) and the resulting reflectivity spectrum (f).

transformation of the depth dependent electron density $\rho(z)$, which is equivalent to the real refractive index,[10] combined with the Fresnel reflectivity $R_F(q_z)$ of a substrate, into a reflectivity of the total structure $R(q_z)$ using:

$$R(q_z) = R_F(q_z)\left|\frac{1}{\rho(\infty)}\int \frac{\mathrm{d}\rho(z)}{\mathrm{d}z} e^{iq_z z} dz\right|^2 , \qquad (8)$$

where the wave vector q_z is defined as:

$$q_z = 2\frac{2\pi}{\lambda}\sin\alpha_i \quad . \qquad (9)$$

This method neglects the absorption and multiple scattering in the structure, and can therefore not be used for quantitative analysis of the multilayer structure. Qualitatively this theory proves to be very useful to explain why the highest reflectivity is achieved for materials that have the largest difference in refractive index. A high contrast will lead to a higher value of the derivative of $\rho(z)$ and immediately results in a higher R.

Another trend easily explained using the Fourier method is the effect of the penetration depth, and thus absorption, on the selectivity of the multilayer mirror. In the Fourier analysis the stack is considered to be semi-infinite, obviously neglecting absorption. The electron density $\rho(z)$ of this stack, as plotted in Figure 6a, can be described with a square wave function $S(z)$. The result after applying the Fourier method is plotted in Figure 6b. This spectrum contains delta peaks at the positions where the Bragg-condition is fulfilled. Due to absorption, the penetration depth of the radiation is not infinite and in a first approximation one could therefore assume that all layers below a certain critical depth do not contribute to the reflected signal while the layers above contribute completely. The effective electron density profile is shown in Figure 6e. Basically, the derivative of the electron density function is multiplied with a rectangle function as shown in Figure 6c. To determine the reflectivity of the resulting profile the reflectivity profile from the semi-infinite stack is thus convoluted with the Fourier transform of the rectangle function, which is a sinc function as shown in Figure 6d. The resulting reflectivity profile is shown in Figure 6f, where each delta peak is replaced with the square of a sinc function (sin(x)/x). This shows that indeed the width of the peaks is increased, and thus the selectivity is decreased, when one limits the number of participating periods. At the same time the reflectivity drops, since the height of the sinc function is proportional to the width of the rectangle function.

1.3.2 Recursive method

To be able to calculate the actual reflectivity of any structure, the Fourier method is not appropriate, since it does not take into account the absorption and multiple reflections in the structure. A method which does take this into account is the recursive calculation method.[15] In this method, the total reflected amplitude r_f of a film on top of another structure is determined by the reflected amplitude r_t of the top interface, to be calculated using eq. (4) and the reflected amplitude r_b of the structure underneath:

$$r_f = \frac{r_t + r_b e^{2i\varphi_i}}{1 + r_t r_b e^{2i\varphi_i}} \quad , \qquad (10)$$

where

$$\varphi_i = \frac{2\pi}{\lambda} \boldsymbol{n}_i d_i \sin\alpha_i \qquad (11)$$

represents the phase delay produced by the propagation of the wave through the ith film with a thickness d_i and a refractive index $\boldsymbol{n}_i$. α_i is the (grazing) angle of the wave within this layer, to be calculated using Snell's law. The reflected amplitude r_b of the structure underneath can recursively be calculated by sub-dividing this structure in another layer on top of the remaining structure, until only one layer on top of the substrate remains. In this last iteration r_b equals the Fresnel reflectivity of the substrate (eq. (4)).
Since this method includes the influence of absorption by means of the complex part of the refractive index $\boldsymbol{n}_i$, it gives the exact solution for structures that can be described using sharp boundaries between all layers.

1.3.3 Matrix method

For structures not consisting of discrete layers (e.g. diffuse boundaries) exact solutions cannot be calculated, and the structures have to be approximated by a series of small layers having sharp boundaries. A good approximation might require over one hundred layers per period, which make the calculation much more complex. In this case the matrix method[16,17], a variant on the recursive method, has proven to be much easier to use since it takes full advantage of the periodic structure of a multilayer mirror. Using this method one relates the forward $E^+(z)$ and backward $E^-(z)$ travelling plane waves on each side of the structure to each other using a 2x2 matrix **S**:

$$\begin{pmatrix} E^+(z) \\ E^-(z) \end{pmatrix} = \begin{pmatrix} S_{11} & S_{12} \\ S_{21} & S_{22} \end{pmatrix} \begin{pmatrix} E^+(z+d) \\ E^-(z+d) \end{pmatrix}, \qquad (12)$$

or

$$\mathbf{E}(z) = \mathbf{S}\mathbf{E}(z+d), \tag{13}$$

where d equals the thickness of the structure. The scattering matrix $\mathbf{S}$ represents the overall reflection and transmission characteristics of the structure and can be composed of a product of the interface and layer matrices $\mathbf{I}$ and $\mathbf{L}$:

$$\mathbf{S} = \prod_{l=1}^{l=N} \mathbf{I}_l \mathbf{L}_l , \tag{14}$$

where N equals the number of layers, $\mathbf{I}_l$ equals the interface matrix between layer l and l-1:

$$\mathbf{I}_l = \frac{1}{t_{l-1,l}} \begin{pmatrix} 1 & r_{l-1,l} \\ r_{l-1,l} & 1 \end{pmatrix} , \tag{15}$$

and $\mathbf{L}_l$ equals the layer matrix of layer l:

$$\mathbf{L}_l = \begin{pmatrix} e^{i\varphi_l} & 0 \\ 0 & e^{-i\varphi_l} \end{pmatrix} . \tag{16}$$

The reflectivity R of the structure can easily be calculated using:

$$R = \frac{E^-(z)}{E^+(z)}, \tag{17}$$

and by taking $E^-(z+d) = 0$ (12) yields:

$$R = \frac{S_{21}}{S_{11}}, \tag{18}$$

The main advantage of this calculation method is the ability to perform fast calculations of systems with many periods, since one can calculate a matrix describing one period, and then raise this matrix to the power of the number of periods to obtain the result for the full multilayer stack.

1.4 Experimental set-up

1.4.1 Hardware

A schematic view of the essential parts of the deposition setup available at the FOM Institute AMOLF (used for this research) is shown in Figure 7. The sample is mounted in a vacuum vessel (base pressure ~1x10^{-9} mbar), and the two materials are sequentially

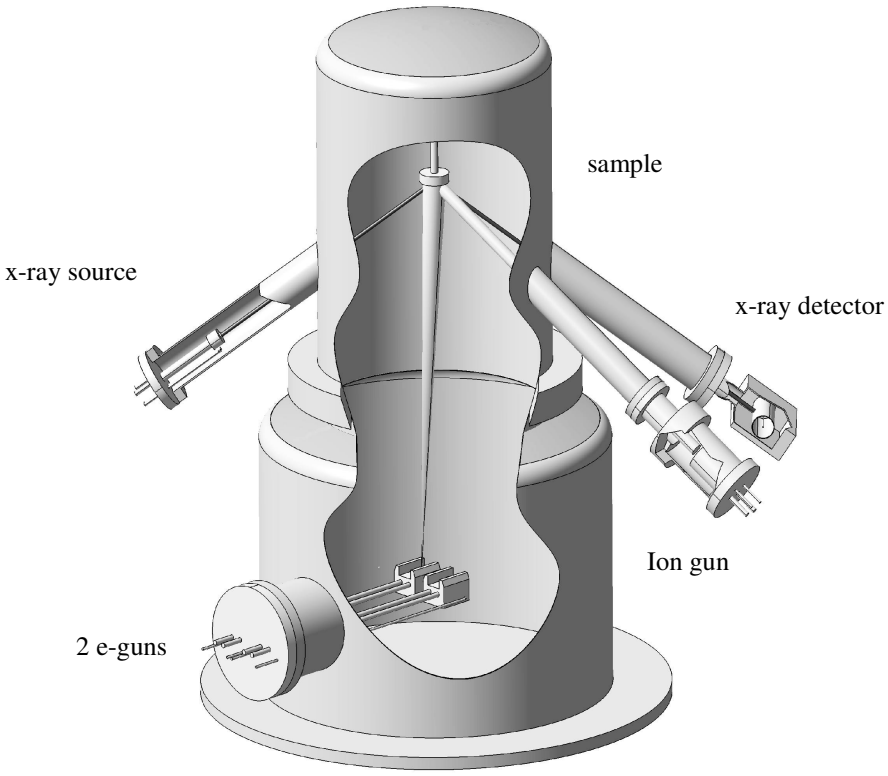

Figure 7 Schematic view of an e-beam deposition setup

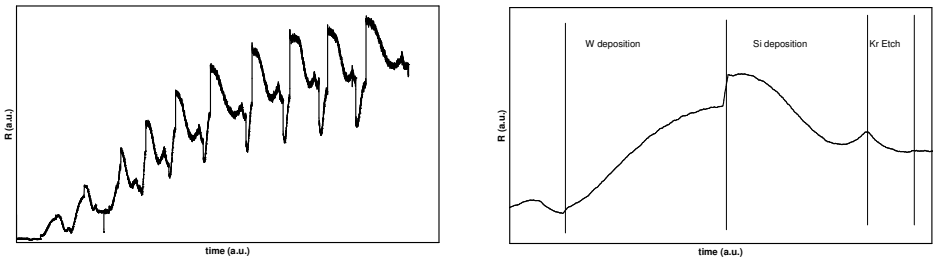

(a) (b)

Figure 8 Measured reflected intensity during the deposition of a 10-period W/Si multilayer mirror (a) and detail of one period, indicating the different process stages (b).

evaporated using two electron guns. It is noted that the deposited layer thickness varies in the lateral direction of the sample due to the cosine-like profile of the particle flux. A method to correct for this error has been developed and demonstrated earlier.[18,19] For the small (1 cm^2) samples produced in the current research this correction did not appear to be necessary.

The thickness of the growing layer can be monitored by measuring the reflected x-ray intensity as a function of the time. An example of such an in-situ growth signal is shown in Figure 8. The optimal thickness of the high δ material (W in this example) is reached when the reflected intensity reaches a local maximum, corresponding to a positive interference between radiation reflected from the surface and from the stack underneath. For the low δ material (i.e. Si) the optimal thickness is reached when the reflected intensity is at a local minimum. If Kr ion beam smoothening is applied to this layer, the layer is deposited with a small excess thickness that is removed by ion beam sputtering.

1.4.2 Software

When performing fundamental research, a lot of parameters have to be varied to be able to determine their influences on the process, a situation obviously requiring flexible, simple and adjustable software to control the deposition process. The computer program, which is written in LabView, is designed such that each physical device relevant for the deposition process is created as a software object. Such an object has then the same controls as the physical device, e.g. for the electron gun these controls are the filament current, electron voltage and emission current. Using these controls the operator can give commands based on the desirable, physical, output. This can be done either manually via the graphical user interface, or completely autonomous via a script. In the latter case a multilayer mirror can, in principle, be grown without attendance of personnel.

1.5 Applications

1.5.1 X-ray microscopy

X-ray microscopes are the short-wavelength analogons of optical microscopes and equally consist of optical elements to collimate the light of a light source onto a sample, and a set of optics for object magnification and imaging. According to Rayleigh's resolution criterion the smallest center-to-center distance Δx between two resolvable objects is:

$$\Delta x = k\frac{1.22\lambda}{NA} \quad , \qquad (19)$$

where *NA* is the numerical aperture of the optical system and *k* an application dependent parameter. This shows the major advantage of x-ray microscopy above visible light microscopy: the achievable resolution is much higher due to the smaller wavelength of x-rays. However, additional requirements needed to form an image of the sample are a high optical contrast between different parts of the sample and, obviously, a sufficient transmission of the radiation through the sample. For example for biological samples, consisting of primarily water and carbon, there exist two regions with sufficient optical contrast between the two materials: in the visible region and in a very small region between the oxygen and the carbon absorption edges (2.4 and 4.4 nm), the so-called water window. The penetration depth of the radiation through water is about 10 μm in the water window, just enough to transmit through a complete cell. This is in contrast for example to electron microscopy, which allows very high resolution images, but also requires the cell to be cut into small slices. X-ray microscopy thus enables high-resolution images of complete and (at the moment of exposure) living cells.

Currently, most soft x-ray microscopes use synchrotron radiation sources. Since the radiation from such a source is nearly monochromatic and has a low divergence, zone plates can be used as collector optics, as well as magnifying optics. However, to make x-ray microscopy a commonly used tool for e.g. biologists, a laboratory-sized microscope (including the source) is required. Therefore several groups are currently developing "table-top" x-ray sources, based on e.g. laser plasma's, discharge plasma's, and Cherenkov radiation. These sources emit the radiation either in cosine-like angular distributions (plasmas) or in a hollow cone in the forward direction with a relative large angle to the central axis (Cherenkov). Due to the large angles at which the radiation is emitted and the physical limitations on the size of zone plates, a zone plate would need to be placed very close to the source, creating difficulties due to the erosive properties of plasmas or energetic electrons. Multilayer mirrors, which are not physically limited in size, are more advantageous in this respect, and allow the collection of a large part of the emitted radiation, even at large distances to the source. For plasma-based x-ray sources the mirrors are also used as monochromator.

The most important property of this collecting optical element is its reflectivity. As can be determined from the Fourier theory, the reflectivity is maximized at maximal optical contrast between the two bi-layer materials. The refractivity index of materials exhibits discontinuities around its absorption edges, which results in a very low β and very low δ at wavelengths just longer than this absorption edge. Scandium is a favorable material for the water window since it has an absorption edge at 3.11 nm.[20] The other material should thus have a high δ and a low β, a condition met by Ni, Cu, Co, Fe, Mn, Cr or V. A recent demonstration of a Cr/Sc multilayer resulted in a reflectivity of 14.5% at 3.11 nm at 2.5

degrees of normal.[21] The major reason for not reaching the theoretical reflectivity of 64% was the interface widths of 0.34 nm, illustrating our findings described in Sect. 1.1.

1.5.2 Extreme UltraViolet Lithography (EUVL)

To be able to produce denser computer memory and faster processor chips, it is required that the critical dimensions of the transistors in these chips are as small as possible. This critical dimension is again determined by Rayleigh's criterion (Eq. (19)) applied to the image forming optical system in lithographic equipment. By consequence, lithography companies continuously reduce the wavelength to create smaller transistors. Currently the first demonstration systems for EUV (13.5 nm) lithography are being producing. Since a lithography tool is basically an inversely used microscope, similar issues as for the x-ray microscopy have to be solved: a compact, bright source has to be found and the multilayer mirrors should have maximized reflectivity.
The wavelength of 13.5 nm has been selected because of its proximity to the Si-L absorption edge. Similar to the material selection for the mirrors in the microscope, this enables the use of Mo/Si multilayer mirrors with a theoretical reflectivity of 74%. A value of 69.5% has been demonstrated in our group.[5] Although this reflectivity seems very high, the total optics transmission is still low (<3%) due to the ten multilayer optical elements that need to be used. Any increase in reflectivity is, commercially, very desirable. Similar to the situation in x-ray microscopy, the multilayer reflectivity is mainly limited due to the non-zero interface widths.

1.5.3 X-Ray Fluorescence spectrometry (XRF)

X-ray fluorescence spectrometry is a non-destructive analytical technique used to identify and determine the concentrations of elements present in solid, powdered or liquid samples. In Table 1 it was described as "photon excites atom, which emits a photon". The use of natural crystals or multilayer elements as the dispersive element is shown in the schematic view of a typical XRF setup in Figure 9. An intense beam of primary x-rays irradiates the sample. Due to the high energy of these x-rays inner shell electrons of the sample's atoms are ejected. This electron vacancy is filled by an electron transferring from predominantly the next higher shell. The energy released during this process is equal to the difference in binding energy of electrons in the two levels, and emitted as a secondary, or fluorescent, x-ray photon. This results in a discrete energy, characteristic of the atom. An overview for all elements emitting radiation between ~1 and 20 nm is shown in Figure 10. This wavelength range is the range in which the low-Z elements emit their fluorescent radiation. By using the selective property of the Bragg crystal or multilayer

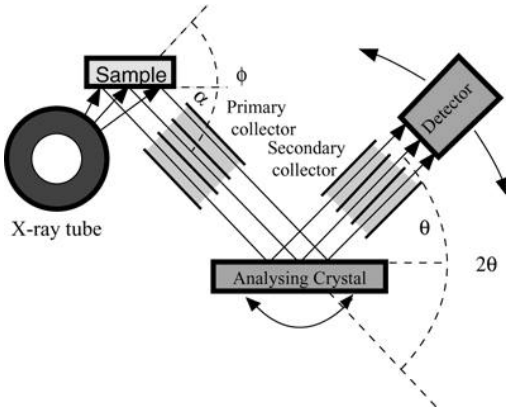

Figure 9 Schematic view of an XRF setup (picture by Norbert Laskowski).

mirror (in this application commonly referred to as artificial crystal) a spectrum of the emitted fluorescent radiation, and thus the present elements, can be measured using an x-ray detector. To be able to discriminate the materials, like N (3.16 nm) and Sc (3.14 nm), a selectivity larger than 150 is required.

Not only the selectivity of the multilayer mirror is of importance for this analysis method, also the reflectivity is important to increase the detection limit (governed by the signal-to

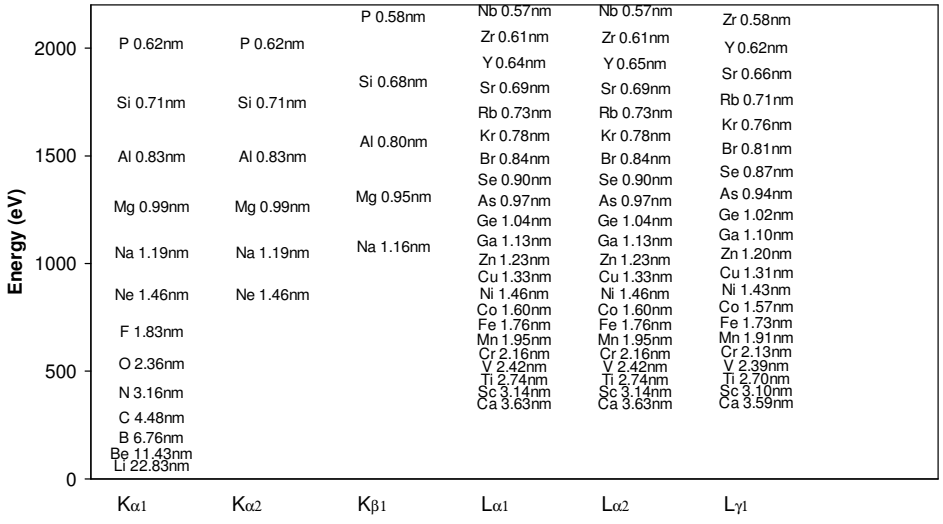

Figure 10 emitted x-rays in the soft x-ray region.

noise ratio). When one mirror is used to analyze more than one element, the mirror should additionally have a wide reflectivity band. This excludes multilayer materials with an absorption edge in that band. A typical example of a multilayer mirror used in an XRF setup is a W/Si multilayer mirror.

1.6 Outlook

The more than 90 years of research after the first pioneering activity of father and son Bragg in the field of x-ray reflecting periodic crystals has led to a large number of viable applications. Multilayer mirrors, which first appeared in 1940,[1] have significantly extended that range of applications. Yet, much important information is still missing, mainly on the fundamental processes occurring during thin (multi-)layer growth. Microscopic models, in particular the numerical growth models employed in molecular dynamics, can only partly provide that information. This is mainly because the lack of computer power necessitates the use of unrealistic process conditions, like for instance a deposition rate of 0.3 m/s.[22] On the other hand, macroscopic models, although very comprehensible, do not include the atomic scale processes. Experimental data obtained so far contained only the average interface widths, e.g. as a function of sample temperature,[23] as function of ion energy[9,24,25] or ion impact angle.[24] The analysis technique presented in chapter 3 will enable the measurement of these effects while distinguishing between the individual interface widths (Chapter 4). Also the origin of degradation of the multilayer mirrors caused by storage, high dose EUV or electron exposure can be investigated in considerably more detail. This enables more fundamental research on the physical and chemical processes occurring within these structures. This then, may result in higher stability, and improved reflectivity of optical elements for x-ray microscopy, EUV lithography, and XRF. For example, if the interface widths of 0.34 nm[21] in the microscopy-relevant Cr/Sc multilayer could be reduced to 0.17 nm, the reflectivity would increase by a factor of 4. This would allow shorter exposure times, preventing radiation damage to appear in the x-ray image. Similar improvements would be possible for XRF applications, resulting in faster materials analysis.

Additionally, the analysis technique presented in chapter 3 would also enable a better understanding of the differences observed between multilayers deposited by e-beam deposition, by magnetron sputter deposition, or pulsed laser deposition. The basic difference between these techniques is that the first is typified by the use of low energy ions at specific moments during the deposition, while in the latter two techniques ions with a broad energy distribution are present during the entire process. Laser deposition is also characterized by high-energy particles, and a large degree of preservation of the

composition of the evaporated material. Effects at deeper layers in the multilayer stacks grown with each of these techniques can then be distinguished in detail. Such research would be an answer to an historic debate among deposition physicists on the advantages and disadvantages of the different deposition methods applied.

The application of hydrogen implantation and subsequent deposition of an adhesion layer (chapter 6) could be applied to Mo/Si multilayer mirrors for EUVL. This would in theory lead to an increase in reflectivity by 1%, resulting in a change of the total transmission of a ten mirror system from 2.6% to 3%, corresponding to a 15% higher production rate in the lithography equipment. This method even enables the application of optically favorable material combinations, which were not yet applied because of low adhesion or island growth.

A last question that emerged from this research concerns the growth of tungsten-rhenium on silicon. Both physically as well as chemically this compound is very similar to pure tungsten, yet the growth is completely different. In-situ scanning tunneling microscopy might be a good tool to study this effect at a true atom-by-atom growth process, with in-situ visualization of the layer topology.[26]

1.7 References

1 J. DuMond and J.P. Youtz, J. Appl. Phys. **11** (5), 357 (1940).

2 R. Schlatmann, A. Keppel, S. Bultman, and J. Verhoeven, presented at the Meeting on Physics of X-ray Multilayer Structures, Jackson Hole, WY, USA, 1994 (unpublished).

3 R. Schlatmann, A. Keppel, S. Bultman, T. Weber, and J. Verhoeven, Appl. Phys. Lett. **68** (21), 2948 (1996).

4 A.A. Fraerman, S.V. Gaponov, V.M. Genkin, and N.N. Salashchenko, Nuclear Instruments and Methods in Physics Research Section A: Accelerators, Spectrometers, Detectors and Associated Equipment **261** (1-2), 91 (1987).

5 E. Louis, A.E. Yakshin, P.C. Görts, S. Oestreich, R. Stuik, M.J.H. Kessels, E.L.G. Maas, F. Bijkerk, M. Haidl, S. Müllender, M. Mertin, D. Schmitz, F. Scholze, and G. Ulm, presented at the Emerging Lithographic Technologies IV, SPIE's 25th Annual International Symposium on Microlithography, Santa Clara, 2000 (unpublished).

[6] S. Braun, H. Mai, M. Moss, R. Scholz, and A. Leson, Japanese Journal of Applied Physics Part 1-Regular Papers Short Notes & Review Papers **41** (6B), 4074 (2002).

[7] Center for X-ray optics, http://www-cxro.lbl.gov/.

[8] E.J. Puik, M.J. van der Wiel, H. Zeijlemaker, and J. Verhoeven, Appl. Surf. Sc. **47**, 251 (1991).

[9] A.E. Yakshin, E. Louis, P.C. Görts, E.L.G. Maas, and F. Bijkerk, Physica B **283** (1-3), 143 (2000).

[10] M. Tolan, *x-ray scattering from soft-matter thin films*. (Springer-Verlag, Berlin Heidelberg New York, 1999).

[11] I.V. Kozhevnikov, Nuclear Instruments & Methods in Physics Research Section a-Accelerators Spectrometers Detectors and Associated Equipment **508** (3), 519 (2003).

[12] R. Jenkins, in *Encyclopedia in Analytical Chemistry*, edited by R.A. Meyers (John Wiley & Sons Ltd., Chichester, 2000), pp. 13269.

[13] J. Kirz, J. Opt. Soc. Amer. **64**, 301 (1974).

[14] F.L. Pedrotti and L.S. Pedrotti, *Introduction to Optics*, 2 ed. (Prentice Hall, 1992).

[15] E. Spiller, (SPIE (Society of Photo-optical Instrumentation Engineers), 1994).

[16] F. Abelés, Annales de Physique **5**, 596 (1950).

[17] R.M.A. Azzam and N.M. Bashara, *Ellipsometry and polarized light*. (North Holland Physics publishing, Amsterdam, 1987).

[18] M.J.H. Kessels, M.Sc., Technische universiteit Eindhoven, 2000.

[19] F. Bijkerk, A.E. Yakshin, E. Louis, M.J.H. Kessels, E.L.G. Maas, and C. Bruineman, USA Patent No. US2004/0052942 A1 (18-3-2004).

[20] B.L. Henke, E.M. Gullikson, and J.C. Davis, Atom. Data Nucl. Data Tables **54** (2), 181 (1993).

[21] F. Eriksson, G.A. Johansson, H.M. Hertz, E.M. Gullikson, U. Kreissig, and J. Birch, Opt. Lett. **28** (24), 2494 (2003).

[22] P. Klaver and B. Thijsse, Thin Solid Films **413** (1-2), 110 (2002).

[23] H.-J. Voorma, E. Louis, N.B. Koster, and F. Bijkerk, J. Appl. Phys. **83** (9), 4700 (1998).

[24] H.-J. Voorma, E. Louis, F. Bijkerk, and S. Abdali, J. Appl. Phys. **82** (4), 1876 (1997).

[25] F. Eriksson, G.A. Johansson, H.M. Hertz, and J. Birch, Opt. Eng. **41** (11), 2903 (2002).

[26] M.J. Rost, D.A. Quist, and J.W.M. Frenken, Physical Review Letters **91** (2), #026101 (2003).

2 Optimal density profile in x-ray multilayer mirrors

2.1 Abstract

It is theoretically shown that infinitely narrow interface layers in multilayer reflective optics in all cases result in the highest reflectivity, at any required selectivity of the multilayer structure.

2.2 Introduction

In various analysis and imaging techniques in the soft x-ray wavelength range, such as x-ray fluorescence analysis,[1] extreme ultraviolet lithography,[2] and x-ray microscopy,[3] multilayer soft x-ray mirrors are applied as reflective or dispersive optical elements. In contrast to the natural crystals alternatively employed for some of these techniques, the synthetically produced multilayer systems in principle can be designed with arbitrary layer periodicity, and arbitrary in-depth density profiles. This provides considerable space for optimization of the reflective and selective characteristics. Most frequently, for instance in extreme ultraviolet lithography, these optimizations concern the mirror's peak reflectivity. It is commonly known that the best reflectivity is obtained in the, theoretical, case of infinitely thin interface layers between the layers of the two multilayer components. This is illustrated by the Debye-Waller factor,[2] which expresses the correction of the reflectivity R_0 of an ideal structure by the loss of reflectivity due to an interface layer with a finite width σ:

$$R(q_z) = R_0 e^{-q_z^2 \sigma^2} \quad , \qquad (20)$$

where the in-depth component of the wave vector q_z is defined as:

$$q_z = 2\frac{2\pi}{\lambda}\sin\alpha_i \quad , \qquad (21)$$

with α_i equalling the grazing angle of incidence and λ the wavelength of the incident radiation. Any increase of the width σ obviously results in a decrease of reflectivity.
However, this interface width also influences other optical multilayer characteristics, like angular selectivity $\theta/\Delta\theta$ or wavelength selectivity $\lambda/\Delta\lambda$, thus allowing several ways of optimisation of these properties. For example, an adjustment of the selectivity by modifying the materials density distributions at the interfaces has been suggested by Fraerman et al.[4] and Schlatmann et al.[5] While the corresponding graded layer distributions have indeed succesfully been demonstrated recently,[6,7] these results now raise a more general question, namely "which profile would result in the highest performance when considering reflectivity and selectivity *simultaneously*", or "is this profile different from the standard multilayer structure having sharp interfaces". As an example, we show a numerical simulation of the reflectivity and selectivity of a structure with exponentially graded densities at the interfaces (Figure 11). The data, plotted as a function of the high-Z material fraction, are compared with that of a standard multilayer having infinitely sharp interface boundaries. From this comparison it follows that at least this specific choice of graded interfaces for no single value of the selectivity resulted in a higher reflectivity as compared to the standard structure. This suggests that the standard structure might always

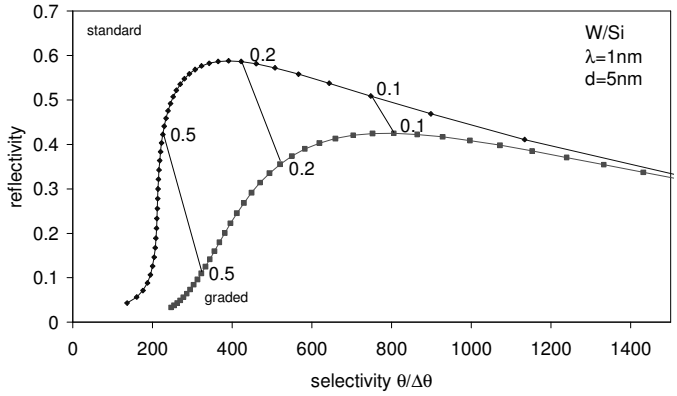

Figure 11 Reflectivity and selectivity as a function of absorber content (indicated by the labels) for a W/Si multilayer mirror with a period of 5 nm and incident radiation with a wavelength of 1 nm. Diamonds: classical structure with sharp interfaces. Squares: structure consisting of periods with one sharp interface and one interface with an exponentially decaying density profile.

result in the best performance. Until now, a globally valid theoretical evidence for this widely accepted proposition was still missing. In this paper this evidence is given.

2.3 Theory

To be able to determine the reflectivity as function of a certain materials density profile, we use the Fourier method.[8] This method allows an analytical solution, based on the transformation of the depth dependent electron density $\rho(z)$, which is equivalent to the density profile, combined with the Fresnel reflectivity $R_F(q_z)$ of a substrate into a reflectivity of the total structure $R(q_z)$ using:

$$R(q_z) = R_F(q_z)\left|\frac{1}{\rho(\infty)}\int \frac{\mathrm{d}\rho(z)}{\mathrm{d}z} e^{iq_z z}\mathrm{d}z\right|^2 . \qquad (22)$$

This method neglects the absorption and multiple scattering in the structure, and therefore it only allows direct comparison of structures having the same absorption within each period, or equivalently, the same integral value of the electron density $\rho(z)$ within each period. The effect of absorption will be considered later on.

2.3.1 Effect of profile on reflectivity

To determine the periodic profile that results in the maximum reflectivity, we start from an arbitrary distribution of two materials, as shown in Figure 12a: a high Z material, having a high contribution to the electron density (dark circles), and a low Z material with a low contribution to the electron density (white circles). This structure is repeated such that a periodic structure is formed. Lateral averaging, i.e. over the x-y plane, results in an arbitrary profile $\rho_1(z)$ as shown in Figure 12b. Our analysis is now aimed at the increase of the reflectivity by modifying this electron density profile. Because the Fourier method does not take absorption into account, we first compare profiles that have the same amount of absorbing material per period. The total electron density is determined by this amount, thus the integral value of the electron density for all profiles is to stay constant. When comparing two profiles, e.g. $\rho_1(z)$ and $\rho_2(z)$, this requirement is formulated as:

$$\int_0^d \rho_1(z)\mathrm{d}z = \int_0^d \rho_2(z)\mathrm{d}z . \qquad (23)$$

Since we are comparing structures with a constant amount of material, the electron density can only be altered by exchanging a high Z material by a low Z material. Therefore we

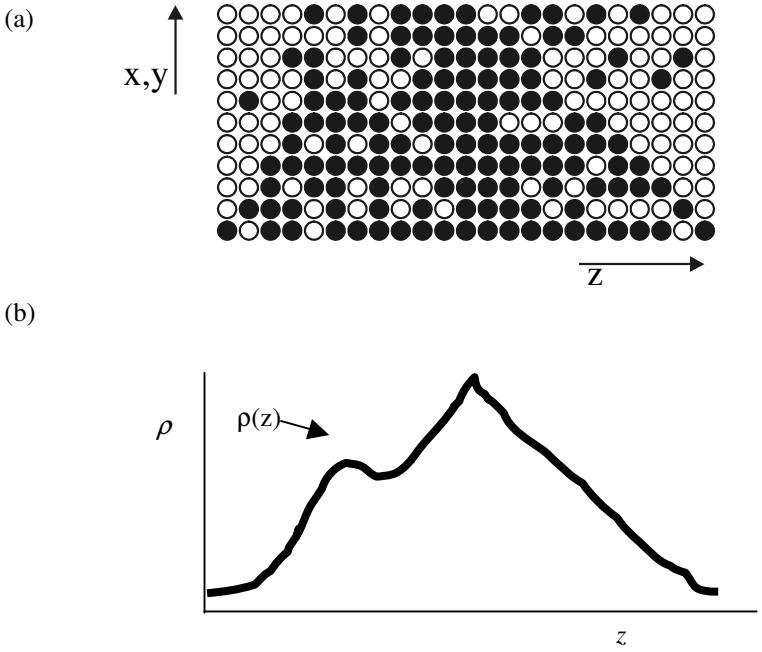

Figure 12 Two-dimensional visualisation of one period of an arbitrary structure consisting of high-Z (black) and low-Z (white) material (a) and its in-depth electron density profile (b).

can approximate the electron density profile also with a sum of block functions, where each block function represents the difference $\Delta\rho$ between the electron density of the low Z material and the high Z material:

$$\rho_1(z) = \rho_{\min} + \sum_{n=0}^{N} B_n(z) . \qquad (24)$$

Each block function $B_n(z)$ thus represents an amount of electrons equal to $\Delta\rho * \Delta z$ located between $z=\varphi_n$ and $z=\varphi_n+\Delta z$, and is mathematically described as:

$$B_n(z) = \begin{cases} \Delta\rho & \varphi_n \le z \le \varphi_n + \Delta z \\ 0 & \text{elsewhere} \end{cases} . \qquad (25)$$

Obviously, the electron density value is between the extreme values of the pure components used in the multilayer structure:[9]

$$\rho_{\min} \le \rho(z) \le \rho_{\max} . \qquad (26)$$

This alternative approximation of the electron density function is visualised in Figure 13 by the use of the blocks. In an amorphous structure, φ_n may have any value.
Substituting (24) in (22) results in:

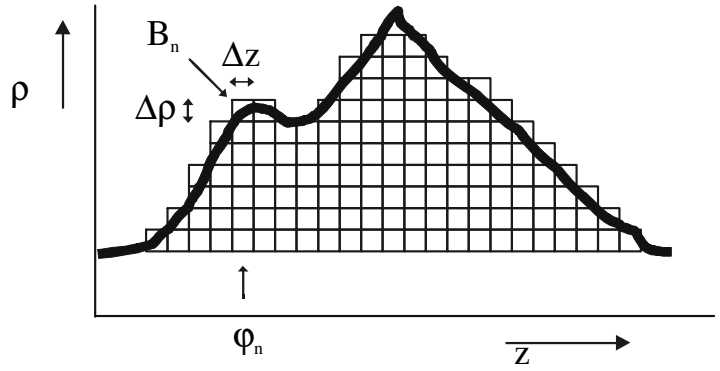

Figure 13 Approximation of the arbitrary density profile of Fig. 2 with a sum of block profiles having a width Δz and a height $\Delta\rho$. By increasing the number of block profiles and simultaneously reducing their width and height the structure can be more accurately described.

$$R(q_z) \approx R_F(q_z)\left|\frac{1}{\rho(\infty)}\int\left(\sum_{n=0}^{N}\Delta\rho\,\delta(z-\varphi_n)-\Delta\rho\,\delta(z-\varphi_n-\Delta z)\right)e^{iq_z z}dz\right|^2 \qquad (27)$$

where $\delta(z-\varphi_n)$ and $\delta(z-\varphi_n-\Delta z)$ are Dirac delta functions. Calculating the integral results in:

$$R(q_z) \approx R_F(q_z)\left|\frac{1}{\rho(\infty)}\sum_{n=0}^{N}\Delta\rho e^{iq_z\varphi_n}-\Delta\rho e^{iq_z\varphi_n}e^{iq_z\Delta z}\right|^2. \qquad (28)$$

For small Δz, we can approximate $e^{iq\Delta z}$ by the first order Taylor expansion $1+iq\Delta z$, which results in:

$$R(q_z) \approx R_F(q_z)\left|\frac{-iq_z\Delta\rho\Delta z}{\rho(\infty)}\sum_{n=0}^{N}e^{iq_z\varphi_n}\right|^2. \qquad (29)$$

From this expression it is obvious that the reflectivity is maximized when the length of the sum of complex unit vectors $e^{iq_z\varphi_n}$ is maximal. This means that in principle φ_n should be the same for all n. Physically this means that all electrons should be located at a depth equal to φ_0. Taking boundary condition (26) into account, we find that the maximum reflectivity is achieved when the difference between φ_0 and φ_n is minimal, resulting in an optimal electron density for all periods which is described by:

$$\rho_{optimal}(z)=\begin{cases}\rho_{\max} & , \quad a<z<b\\ \rho_{\min} & , \quad z\,\text{elsewhere}\end{cases} \qquad (30)$$

with a and b chosen such that requirement (23) is satisfied. Equation (30) describes a block function, and from this result we conclude that there will be no other profile with the same electron density per period, or equivalently the same absorber fraction per period, for which the reflectivity exceeds the reflectivity of this block profile of the two pure materials.
However, changing the profile into a block profile results in a concentration of absorbing material closer to the nodes of the standing wave formed by the incident and reflected radiation. This leads to a reduction of the absorption,[2] and thus a higher penetration depth of the radiation. As a result, an additional increase of the reflectivity occurs since layers located deeper in the stack now also contribute to the reflected intensity. Thus, even though this change of the absorption is in conflict with the earlier requirement of a constant absorption (needed for the Fourier analysis), the highest reflectivity is still obtained for an electron density profile described by a block function.

2.3.2 Effect of profile on selectivity

When changing an arbitrary profile into a block profile, while keeping the absorber fraction constant, two effects occur that have an opposite effect on the penetration depth of the radiation. On the one hand, the increased reflectivity depletes the incoming beam, effectively causing a decrease of the penetration depth. On the other hand, the localisation of the absorber (see above) results in a reduced absorption causing an *increase* of the penetration depth. According to Frearman[4], who refers to these two effects, the increase of the selectivity due to enhanced concentration of absorber material at the wave nodes only exceeds its decrease due to the higher reflectivity, when the imaginary parts (absorption is dominant) of the refractive indices of the components differ more than the real parts (reflection is dominant). Therefore, we consider two cases: one for which the selectivity decreases when changing the arbitrary profile to the block profile, and one for which the selectivity increases.

2.3.2.1 Selectivity decreases

For this case the transition from the arbitrary profile to the block profile results in a higher reflectivity and lower selectivity (as is shown in Figure 11). If we are able to additionally find a block profile that has a higher selectivity and higher (or equal) reflectivity as the initial arbitrary profile, and if we take into account that changing the absorber fraction results in a monotonous change in the selectivity and a continuous change of the reflectivity with only one maximum, then also a block profile exists which has a higher reflectivity at the same selectivity as the initial arbitrary profile. To accomplish this, we decrease the amount of the absorbing component of the system in the block profile until

the reflection of one single period is the same as for the arbitrary profile. The depletion of the incoming beam due to the reflection is now the same as for the arbitrary profile. Additionally, absorption will not only decrease due to a reduced amount of absorbing material, but also due to further localisation of the absorber material towards the nodes of the standing wave within the multilayer structure. The depletion of the beam due to absorption is now lower than in the case of the arbitrary profile, so the net result will be that more and deeper interfaces will contribute to the reflected intensity, improving the total reflection of the multilayer structure as well as the selectivity. This results in a block profile having a higher reflectivity and selectivity than the initial arbitrary profile. Therefore, also a profile exists which has a higher reflectivity at the same selectivity as the initial profile.

2.3.2.2 Selectivity increases

For the second case, and starting from the earlier found block profile having a higher reflectivity and in this case also a higher selectivity as the initial arbitrary profile, we now have to find a second block profile which has a higher (or at least equal) reflectivity, but lower selectivity. This can be achieved by increasing the absorber fraction in the block profile. This will cause a decrease of the reflectivity per period, and consequently a reduction of the total reflectivity, due to the higher fraction of absorbing material as well as the increased delocalization of this material. Also the penetration depth, or equivalently the selectivity is influenced by two oppositely acting effects, namely an increase of the selectivity due to the reduced reflectivity and a reduction of the selectivity due to the higher absorption. However, since absorption dominates in this case, the latter effect will be stronger than the first. If we choose to increase the absorber fraction such that the resulting total reflectivity is equal to the reflectivity of the initial arbitrary profile, we have found a structure with a lower selectivity at the same reflectivity as the initial arbitrary profile. Again taking into account that the change of the absorber fraction in the block profile results in a continuous change of reflectivity and selectivity, this also shows that a profile exists with the same selectivity but higher reflectivity as the arbitrary profile.

The argumentation above qualitatively shows that for both cases (2.3.2.1 and 2.3.2.2) there will always be a periodic block profile having a higher reflectivity than a periodic arbitrary profile for any selected selectivity.
It is noted that the actual value of the reflectivity and selectivity remains to be determined using numerical methods, like the recursive method[2] or the matrix method.[10,11] This then enables one to select the proper ratio between the thicknesses of the two materials used in the structure. It is also noted that the proof given here is valid only for two-material

multilayer structures. Structures consisting of more than two materials,[12] structures in which the periodicity varies across the multilayer stack,[13] or super-lattices[2] are not dealt with in this treatment.

2.4 Conclusion

It has theoretically been shown that multilayer structures with infinitely narrow interface layers between the two constituent materials in all cases result in the highest reflectivity at any selected selectivity. Therefore, it is in all cases favourable to create a multilayer structure with sharp interfaces. Practical limitations on the achievable interface thickness may favour gradients in the density profile of the multilayer.

2.5 Acknowledgements

This work is carried out as part of the research programme of the Stichting voor Fundamenteel Onderzoek der Materie (FOM) with financial support from the Nederlandse Organisatie voor Wetenschappelijk Onderzoek (NWO).

2.6 References

1 R. Jenkins, in *Encyclopedia in Analytical Chemistry*, edited by R.A. Meyers (John Wiley & Sons Ltd., Chichester, 2000), pp. 13269.

2 E. Spiller, (SPIE (Society of Photo-optical Instrumentation Engineers), 1994).

3 A.G. Michette, Rep. Prog. Phys. **51** (12), 1525 (1988).

4 A.A. Fraerman, S.V. Gaponov, V.M. Genkin, and N.N. Salashchenko, Nuclear Instruments and Methods in Physics Research Section A: Accelerators, Spectrometers, Detectors and Associated Equipment **261** (1-2), 91 (1987).

5 R. Schlatmann, A. Keppel, S. Bultman, T. Weber, and J. Verhoeven, Appl. Phys. Lett. **68** (21), 2948 (1996).

6 This thesis: chapter 5, M.J.H. Kessels, J. Verhoeven, A.E. Yakshin, F.D. Tichelaar, and F. Bijkerk, Nucl. Instrum. Meth. B **222** (3-4), 484 (2004).

7 This thesis: chapter 4, M.J.H. Kessels, F.D. Tichelaar, J. Verhoeven, and F. Bijkerk, (to be published, 2004).

8 M. Tolan, *x-ray scattering from soft-matter thin films*. (Springer-Verlag, Berlin Heidelberg New York, 1999).

9 This restriction is not valid when applying super-lattices

[10] F. Abelés, Annales de Physique **5**, 596 (1950).
[11] R.M.A. Azzam and N.M. Bashara, *Ellipsometry and polarized light*. (North Holland Physics publishing, Amsterdam, 1987).
[12] J.I. Larruquert, Optics Communications **206** (4-6), 259 (2002).
[13] C. Morawe, J.C. Peffen, and I.V. Kozhevnikov, J. Phys. IV **104**, 239 (2003).

3 Determination of in-depth density profiles of multilayer structures

3.1 Abstract

We developed and demonstrate an analysis method in which we calibrate the intensity scale of Cross-Sectional Transmission Electron Microscopy (CS-TEM) using CuKα reflectometry. This results in quantitative in-depth density profiles of multilayer structures. Only three free parameters are needed to obtain the calibrated profiles, corresponding to three CS-TEM image intensity levels, namely the optical indices of the two multilayer materials used and the assumption that the layers are laterally homogeneous. The power and the general usefulness of the method is demonstrated using experimental data of W/Si and Mo/Si multilayer systems with sharp interfaces as well as multilayers of which the interfaces were deliberately intermixed.

3.2 Introduction

Multilayer structures are used in a variety of fields, e.g. extreme ultraviolet lithography,[1] x-ray fluorescence analysis,[2] and vertical cavity surface emitting lasers.[3] In view of the optical application of such structures, especially the density profile, including information on layer intermixing, interface roughness and the distribution of the components is crucial. To be able to properly investigate these structures, extensive analysis of the produced structures should be performed. Available analysis tools based on depth profiling using energetic ions, like auger electron spectroscopy, x-ray photoelectron spectroscopy, as well as secondary ion mass spectroscopy, may induce changes of the original profile. This can be due to intermixing or preferential sputtering.

Microscopic techniques like bright field Cross-Sectional Transmission Electron Microscopy (CS-TEM) are less destructive, but produce an image that is difficult to translate into a quantitative profile. On the other hand, non-destructive techniques based on reflectivity measurements like ellipsometry and x-ray reflectometry, suffer from the so-called inversion problem or phase problem: it is impossible to unambiguously determine the structure from the measured spectrum.[4,5] As a solution, these data usually are subsequently processed by fitting an empirically determined model to the measured reflectivity spectrum. The free parameters to be fitted are for example individual layer thicknesses, material concentrations, interface structures and interlayer thickness. However, the use of such a large amount of free parameters and the implicit information contained in the model reduces the reliability of the fit, even when a perfect match between experiment and fit is found. This is due to the fact that in practice no single model is able to comprehensively describe all physical phenomena, and that different parameters in the model can have a similar effect on the reflectivity spectrum.

Aschentrup et al.[6] demonstrated a method in which they reduced the number of free parameters by determining the layer thicknesses from CS-TEM images. Although this improves the reliability of the result, it still heavily depends on the implicit information contained in the model used to describe the expected structure. In the method we propose here, we will determine the in-depth density profile without using such a model. For this, we obtain an in-depth density profile from a CS-TEM image. This density scale is then calibrated by fitting a simulated reflectivity spectrum determined from the CS-TEM profile to a measured spectrum. Essential data required for this scale are average density (obtainable from the measured critical angle), and optical contrast between the two materials (obtainable from the measured height and shape of the first order Bragg peak after the average density has been determined). Though this not necessarily results in a perfect fit, the resulting in-depth density profile is considerably more reliable than the alternatives described above.

As a result, more complete information, also including layers with different densities and their position is obtained. Since this method does not use any other, implicit data than the CS-TEM image, the actual reflectometry data, the refractive indices of the two, pure, materials in the multilayer structure and the assumption that the layers are laterally homogeneous, the outcome of the method represents a unique description of the structure.

Several merit functions have been tested to find the optimal fit, and both a logarithmic and a linear fit were used. Additionally we added the option to include a weighting of the fit for instrumental errors. Although the fits were affected by the choice of the merit function, the results of the total analysis did not change significantly. This demonstrates the stability of this method.

The power of this method as well as the applicability of the analysis is demonstrated for several deposited multilayers having different interface structures.

3.3 Method

CS-TEM images visualize the intensity of the transmitted electron beam through a structure of typical 20 – 100 nm thickness. To be able to determine the material concentrations from such an image, we first need to formulate the dependency between these two physical properties.

Because of the symmetry in the deposition setup, we can assume that the structure is homogeneous in the direction of the electron beam. For a high reflective coating, the multilayer has to be composed of materials with a large difference in refractive index. In general this means that one material has a high atomic number *Z*, whereas the other material has a low *Z*. According to the scattering contrast theory for amorphous specimens in bright field mode as formulated by Reimer,[7] we can describe the transmission of electrons *T* as an exponentially decaying function depending on the product of density ρ and thickness *t*:

$$\ln(T) = -\beta \frac{Z^{\alpha}}{A} \rho t \quad , \tag{31}$$

where α and β are aperture- and energy-dependent constants and *A* is the atomic mass. The transmission through a mixture of a high-Z material and a low-Z material in a depth-dependent ratio of $C_{\text{high}}(z)$: 1-C_{high}(z), where *z* is in the direction normal to the surface of the multilayer sample, can thus be described as:

$$\ln(T(z)) = -\beta \frac{\left(Z_{\text{high}}\right)^{\alpha}}{A_{\text{high}}} \rho_{\text{high}} t C_{\text{high}}(z) - \beta \frac{\left(Z_{\text{low}}\right)^{\alpha}}{A_{\text{low}}} \rho_{\text{low}} t \left(1 - C_{\text{high}}(z)\right) \tag{32}$$

This can be rewritten as:

$$T(z) = p\, e^{-kC_{high}(z)}, \tag{33a}$$

where

$$p = e^{-\beta \frac{(Z_{\text{low}})^{\alpha}}{A_{\text{low}}} \rho_{\text{low}} t}, \tag{33b}$$

and

$$k = \beta \frac{\left(Z_{\text{high}}\right)^{\alpha}}{A_{\text{high}}} \rho_{\text{high}} t - \beta \frac{\left(Z_{\text{low}}\right)^{\alpha}}{A_{\text{low}}} \rho_{\text{low}} t\,. \tag{33c}$$

When we assume that the imaging system (e.g. film, scanner, camera, etc) has been operated within a linear range, the measured intensity I depends on the transmission T according:

$$I(z) = aT(z) + b\,, \qquad (34)$$

where a is related to the optical quality of the imaging system (e.g. brightness or contrast) and b corresponds to the measured background intensity for which the beam is completely blocked. Using (33a) this results in a dependence of the measured intensity to the concentration of the high-Z material according to:

$$C_{High}(z) = -\frac{\ln\left(\frac{I(z)-b}{a\,p}\right)}{k}\,. \qquad (35)$$

In case we have areas in the CS-TEM image that correspond to non-intermixed zones we can determine from the CS-TEM image an intensity I_{max}, which corresponds to 0% of high-Z material as well as an intensity I_{min} which corresponds to 100% of the high-Z material, the product of a and p can be replaced by I_{max}-b and k by -ln((I_{min} –b)/ (I_{max} –b)), which results into:

$$C_{High}(z) = \frac{\ln\left(\frac{I(z)-b}{I_{max}-b}\right)}{\ln\left(\frac{I_{min}-b}{I_{max}-b}\right)}\,. \qquad (36)$$

Equation (36) contains, in principle, only *one* free parameter (b), which is to be determined by a fit to $\theta/2\theta$ reflectometry data.

In structures that do not contain layers of 100% of high-Z material or layers containing 0% of high-Z material, the intensities I_{min} or I_{max} cannot be determined directly from the TEM image and have therefore to be introduced as additional free parameters. Even when the structures do contain layers with 100% or 0% of high-Z material, the intensity can be higher than I_{max} or lower than I_{min}, due to noise in the acquired CS-TEM image. This also necessitates introducing these two boundaries as additional free parameters. Intensities that are above I_{max} or below I_{min} are then put equal to the respective boundary.

Thus, these three parameters enable us to convert the depth-dependent intensity of the CS-TEM image into a depth-dependent density of the two materials in the structure. This can be used to calculate the angle dependent reflectivity $R_{calculated}(\theta)$, e.g. with the matrix method, which results in the reflectivity using the propagation of the electric field in the

structure.[5,8] Using a fitting algorithm we can change the free parameters in such a way to minimize one of the merit functions M as described by:

$$M_{\text{linear}} = \int_{\theta_{\min}}^{\theta_{\max}} \left(R_{\text{measured}}(\theta) - R_{\text{calculated}}(\theta)\right)^2 \mathrm{d}\theta \qquad (37a)$$

$$M_{\text{weighted linear}} = \int_{\theta_{\min}}^{\theta_{\max}} \left(\left(R_{\text{measured}}(\theta) - R_{\text{calculated}}(\theta)\right) \cdot R_{\text{measured}}(\theta)\right)^2 \mathrm{d}\theta \qquad (37b)$$

$$M_{\text{logartithmic}} = \int_{\theta_{\min}}^{\theta_{\max}} \left(\log\left(R_{\text{measured}}(\theta)\right) - \log\left(R_{\text{calculated}}(\theta)\right)\right)^2 \mathrm{d}\theta \qquad (37c)$$

$$M_{\text{weighted log.}} = \int_{\theta_{\min}}^{\theta_{\max}} \left(\left(\log\left(R_{\text{measured}}(\theta)\right) - \log\left(R_{\text{calculated}}(\theta)\right)\right) \cdot R_{\text{measured}}(\theta)\right)^2 \mathrm{d}\theta \qquad (37d)$$

where $R_{\text{measured}}(\theta)$ is the measured reflectivity curve, $\theta_{\min}$ is equal to the lowest measurable (grazing) angle and $\theta_{\max}$ is the largest angle in the measured range still at a reasonable signal level.

As fitting algorithm we used CFSQP (C code for Feasible Sequential Quadratic Programming), developed by Craig Lawrence, Jian L. Zhou, and André L. Tits,[9,10] which is a set of C functions for the minimization of the maximum of a set of smooth objective functions.

3.4 Reflectivity measurement

We now proceed to determine the minimal required angular range in the Cu-Kα reflectivity measurements. Basically, a reflectometry spectrum $R(q_z)$ is in first order approximation equal to the Fourier transformation of the depth dependent electron density $\rho(z)$ combined with the Fresnel reflectivity $R_F(q_z)$ of a substrate according to:[4]

$$R(q_z) = R_F(q_z)\left|\frac{1}{\rho(\infty)}\int \frac{\mathrm{d}\rho(z)}{\mathrm{d}z} e^{iq_z z} dz\right|^2 \quad , \qquad (38)$$

where the wave factor q_z is defined as:

$$q_z = 2\frac{2\pi}{\lambda}\sin\alpha_i \quad , \qquad (39)$$

with α_i equalling the grazing angle of incidence and λ the wavelength of the incident radiation. From (38), we can see that low frequency changes in the electron density, as

observed in the CS-TEM material density profile, will appear at small grazing angles (low q_z) in the reflectometry measurements. High frequency changes will be seen at larger grazing angles.

We recall that the missing parameters to determine the intensity-to-density scale of the CS-TEM profile are I_{max}, I_{min} and b, which only influence the average density and the maximal optical contrast between the two materials. The average density δ is a constant value, and will thus influence the reflectivity only at very grazing angles. This is also expressed in the approximation for the critical angle θ_c:[1]

$$\sin\theta_c = \sqrt{2\delta} \,. \qquad (40)$$

For periodic multilayer structures, the amplitude of the optical contrast between the two materials should be contained within the height and shape of the first order Bragg peak. Therefore, a fit of a reflectivity measurement including the critical angle and the first order Bragg peak is sufficient to acquire the desired calibration of the CS-TEM data.

To be able to include layer thickness variations, which cause a deviation of the periodicity of the structure and thus influences reflectivity measurement primarily at larger angles, one should include higher orders in the fitting routine. However, since the layer thickness variations are detectable in the CS-TEM picture, they are in principle already taking into account.

It is noted that an extension of the q-space analysis to much larger q-values than up to the first or second Bragg peaks would not necessarily increase the accuracy of the method. This is due to the fact that CS-TEM basically represents a 2D projection of a sample with finite thickness. High-resolution features, corresponding to higher orders in the reflectometry data, are therefore usually not visible. The minimally measured angular range in the reflectivity spectrum should thus at least include the critical angle and the first order Bragg peak. Inclusion of higher angles may add to the accuracy, but most emphasis should be put on the more grazing angles for our CS-TEM intensity scaling purpose.

3.5 Experimental

We prepared all multilayers used for demonstration of the method by e-beam evaporation in an ultra high vacuum system (base pressure 10^{-9} mbar). The thickness of the components was controlled by in situ reflection of C K radiation having an angle with the sample surface of 35°. This technique also provides information on the roughness development of the sequential interfaces. The samples consisted of nine, ten or 50 periods. The material combinations W/Si and Mo/Si were used. W/Si is known to form graded

interfaces under ion bombardment,[11] whereas Mo/Si is known to form silicides[12] under ion bombardment. For this reason we investigated samples with and without Kr^+ ion bombardment of the high-Z material. Additionally, energetic Kr^+ ions were applied to all Si layers to reduce the interface roughness between the components.

The samples were characterized by $\theta/2\theta$ reflectometry at CuKα wavelength (0.154 nm) using a Philips X'pert reflectometer. TEM cross-sectional specimen were prepared by sawing and mechanical polishing to ~ 20 µm thickness, followed by ion milling (Gatan PIPS model 691). Putting the specimen in the edge-on position in the TEM was done with the help of the substrate orientation. The photographs were digitized at 1500 dpi (Nikon super coolscan 8000 ED film scanner). Intensity profiles obtained from line scans perpendicular to the multilayer structure were averaged over a length of 10 nm parallel to the multilayer structure.

Although the thickness T of the multilayer stack can be determined from the CS-TEM images, a small optimization (within 1%) allowed us to obtain a much higher precision than is possible using data from the CS-TEM image only (1%). This is a fourth free parameter T in the total model. In principle one can obtain this value also by analysis of position of the higher order Bragg peaks.[1] However, to be able to measure these high orders a multilayer with a high number of periods is required. The error in the determination of the total thickness is then equal to the error in the period thickness multiplied with the number of periods. This value is generally larger than obtainable by the optimization proposed here.

3.6 Results

Our first application of the method is on a W/Si multilayer of which only the Si surface was smoothened by energetic ions. From the CS-TEM image (Figure 14a) an intensity profile of the multilayer was extracted and averaged as described above (Figure 14b).

By fitting the calculated reflectivity, determined from the CS-TEM intensity profile, to the measured CuKα reflectometry data, as shown in Figure 15a by a thick line, the four free parameters (I_{min}, I_{max} , b and T) are then determined. The result of the optimization of the merit function M_{linear} (Eq. (37a)) is indicated by a solid line. The density profile resulting from this fitting procedure is shown in Figure 15b. Although the fits were affected by the choice of the merit function, the final density profile did not change significantly. Since the linear fit puts more weight on the more grazing angles, which, as discussed above, include information about layer thicknesses and average composition, we preferred this merit function.

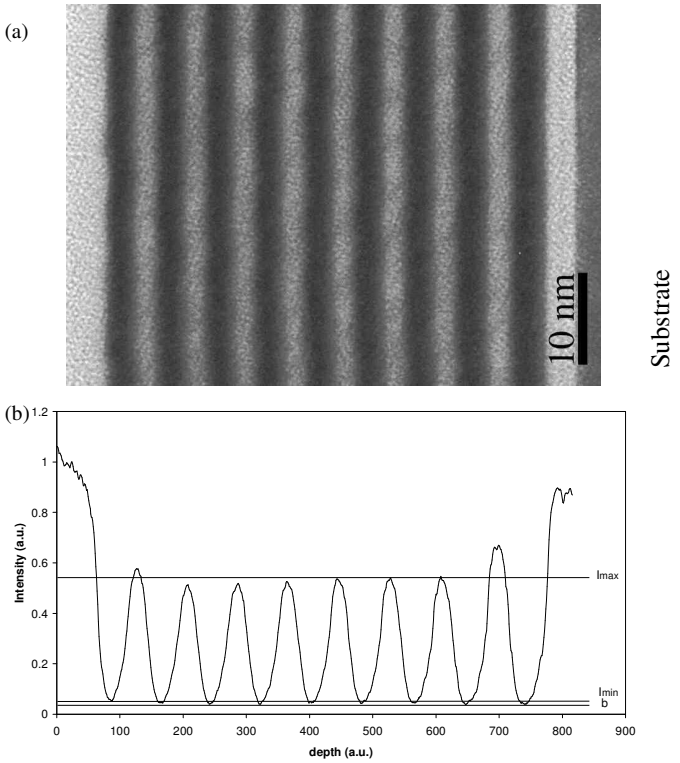

Figure 14a CS-TEM image of a 9 period W/Si multilayers with period thickness of 5.9 nm. After deposition of each Si layer a smoothing procedure with 300 eV Kr+ ions was applied.

Figure 14b Averaged intensity profile as obtained from the top 10 nm of the CS-TEM. Indicated are the levels of I_{max}, I_{min} and *b,* determined from the fitting routine.

The good agreement observed up to the second order diffraction peak demonstrates that period thicknesses as well as individual layer thicknesses and densities are estimated correctly. Small errors in the density profile within each period may cause a deviation of the calculated reflectivity from the measured data beyond the second order Bragg peak. However, the slightly asymmetric shape might still be used to get a good impression of the density profile of a single period, as shown in Figure 15c, and this asymmetry can be explained by diffusion of W into Si.

A similar procedure has been conducted for a second W/Si multilayer, where all but one W layer was completely intermixed into Si. This was achieved by depositing a full period of Si and a half period of W, followed by ion bombardment with 1000 eV Kr^+ ions until the extra half period was removed. As a result, most of the W was removed, but a part of

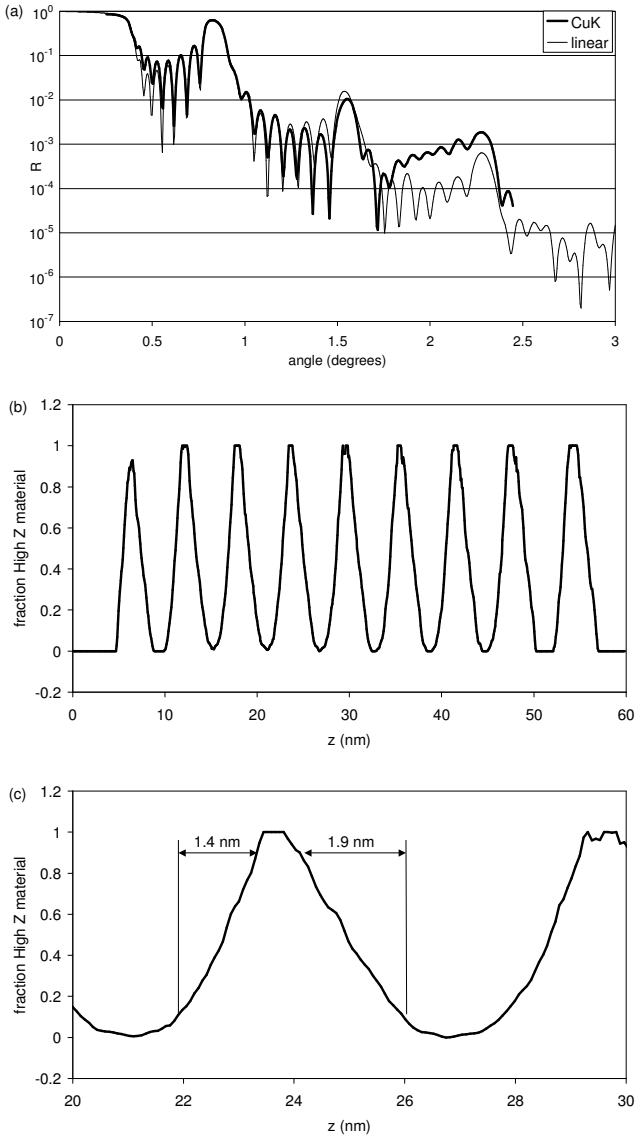

Figure 15 a Measured (thick line), and fitted (thin line) θ:2θ reflectivity curves at 0.154 nm (CuKα).

Figure 15b Tungsten concentration profile of the full multilayer stack as obtained from the cross sectional TEM after calibration of the density and depth scale using the fitting algorithm.

Figure 15c Detail of Figure 15b: tungsten concentration profile of the 4th period. Indicated are the determined interface widths of the Si-on-W interface (1.4 nm) and the W-on-Si interface (1.9 nm)

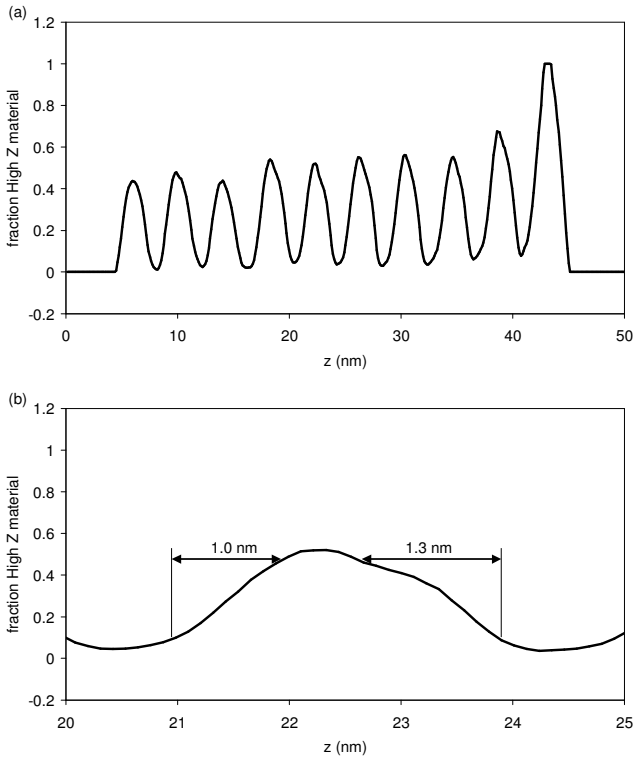

Figure 16a Calibrated tungsten concentration profile of the full multilayer stack. Clearly visible is the difference between the first (deepest) W layer, which is not treated with ions, and the subsequently deposited layers, which are treated with 1000 eV Kr^+ ions.

Figure 16b Detail of Figure 16a: tungsten concentration profile of the 4th period as determined by the fitting algorithm. Indicated are the widths of the Si-on-W interface (1.0 nm) and the W-on-Si interface (1.3 nm)

the W was driven into the Si. Figure 16a shows the density profile of the entire stack, which shows the different first W layer (not intermixed) and the subsequent intermixed periods. The strong asymmetric shape of the density profile of each intermixed period (Figure 16b) indicates an in depth variation of the W concentration caused by intermixing.

As a third example, a Mo/Si multilayer was analyzed. In contrast with the W/Si system, Kr^+ions of 300 eV were sufficient to perform intermixing of Mo into Si. A striking difference with the W/Si structure is that we do not observe a significantly asymmetric shape within each intermixed period in the density profile (Figure 17a and b), which suggests that Mo intermixes with Si only in a constant ratio: the Mo concentration of approximately 40% in the intermixed periods corresponds to $MoSi_2$ [13] (Mo content 38%).

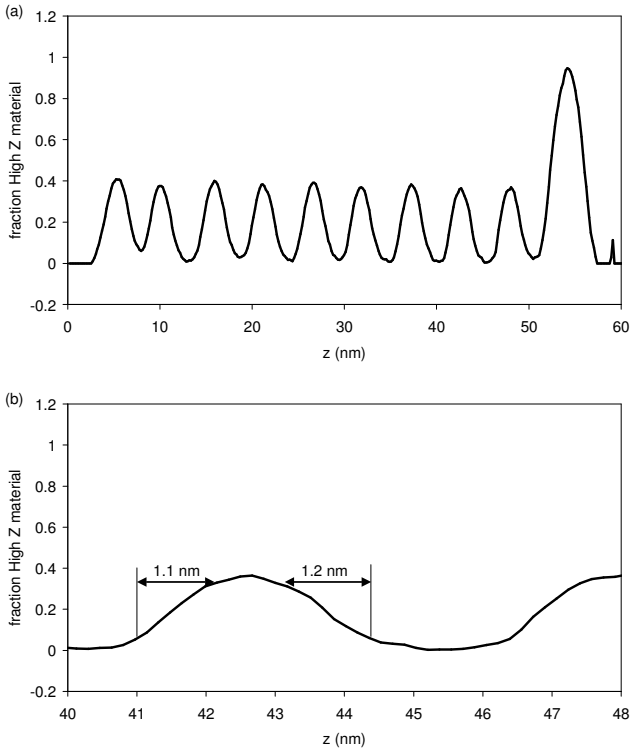

Figure 17a Calibrated molybdenum concentration profile of the full multilayer stack. Also in this figure the difference between the untreated first Mo layer and the subsequently treated Mo layers is visible. Figure 17b Detail of Figure 17a. Molybdenum concentration profile of the 8th period as determined by the fitting algorithm. No significant difference is observed between the Si-on-Mo interface and the Mo-on-Si interface.

As a last example we show data of a 50 period standard Mo/Si multilayer, as generally used in EUV lithography. In this multilayer mirror the Mo layer was not treated with ions. From the CS-TEM image we could determine that small crystallites were present within the Mo layers. Because crystallites appear darker in the CS-TEM image, the minimal intensity in the CS-TEM is too low in this case. However, because I_{min} is a free parameter in the fitting routine, this will not result in an incorrect determination of the intensity of an amorphous Mo layer. The CuKα reflectometry measurement is shown in Figure 18a (thick line, for clarity only a moving average of the measurements is shown; the analysis has been performed on the complete, unaveraged, spectrum). The high reflected intensity of this sample enables more Bragg peaks to be applied in the fitting routine. The results for the linear fit (thin line) as well as the logarithmic fit (dotted line) are shown.

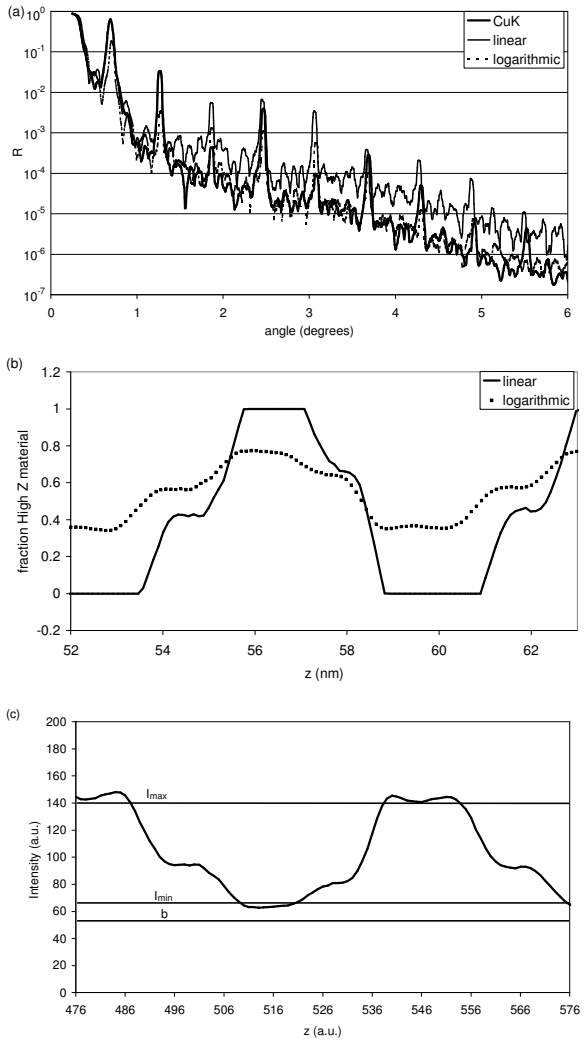

Figure 18a Measured (thick line), linear fitted (thin line) and logarithmic fitted (dotted line) θ:2θ reflectivity curves at 0.154 nm (CuKα) of a 50 period Mo/Si multilayer (period thickness 7.2 nm). For clarity a 9-point moving average of the data is shown. Best agreement at small angles is visible for the linear fit, and at large angles the logarithmic fit shows a better agreement. The Si layers were smoothed by Kr+ ions.

Figure 18b Molybdenum concentration profile of the 8th period as determined by the linear fitting algorithm (solid line) and logarithmic algorithm (dotted line).

Figure 18c TEM intensity profile of the 8th period used to determine the concentration profile. Indicated are the determined levels of the three missing parameters using the linear fit.

For the linear fit the d-spacing was not estimated perfectly as we can observe from the small difference in position with respect to the measured data of the higher order Bragg peaks. Although we observe a relatively good agreement between the fitted result and measurement up to the second order, for larger angles a deviation is visible. This is in contrast to the result of the logarithmic fit for which the larger angles agree well. These deviations are caused by a wedged shape of the TEM sample, causing a gradual change of the observed density. Although the shape of the two determined profiles is similar (Figure 18b), the logarithmic determined profile (dotted line) shows an apparently incorrect $Mo_{75}Si_{25}/Mo_{35}Si_{65}$ structure as compared to the Mo/Si structure determined using the linear fit (solid line).
Because the essential information is provided in the more grazing angles, we conclude that the linear fitting results in a better agreement with the measured data. The density profile determined by linear fit clearly shows two interlayers in each period (Figure 18b). These interlayers were already visible in the original TEM data as can be seen in Figure 18c. Using our method we are now able to determine the absolute concentrations at these interlayers. At the Si on Mo interface a Mo concentration of about 40% is observed, whereas on the Mo on Si interface a Mo concentration of about 70% is visible. This is in good agreement with the Mo concentrations in $MoSi_2$ (35%) and Mo_5Si_3 (69%) found in earlier investigations.[14]

3.7 Discussion

Because the determined density profiles were mostly insensitive for the choice of the merit function, and thus insensitive for the quality of the fit, these examples already give a good indication that the derived density profiles also correspond with the actual structures. However, as with any CS-TEM analysis, an improper alignment of the substrate relative to the electron beam would reduce the quality of the images, notably at the interfaces. When we take into account a maximal CS-TEM sample thickness of 100 nm and a misalignment of maximal 1°, a blurring of 1.7 nm can occur. In that case higher order Bragg peaks loose importance in the fitting procedure. A similar effect is caused by the procedure to obtain the intensity profiles by averaging the CS-TEM pictures. Figure 19a shows the result of the analysis of the CS-TEM input profile of the 10-period W/Si multilayer where this profile has been blurred using a 2 nm wide averaging (dotted line). The previously determined profile has been included for reference (solid line). Due to the averaging, details with a scale below 2 nm are removed. The calculated reflectivity for both profiles is shown in Figure 19b. Clearly visible is the perfect agreement around the

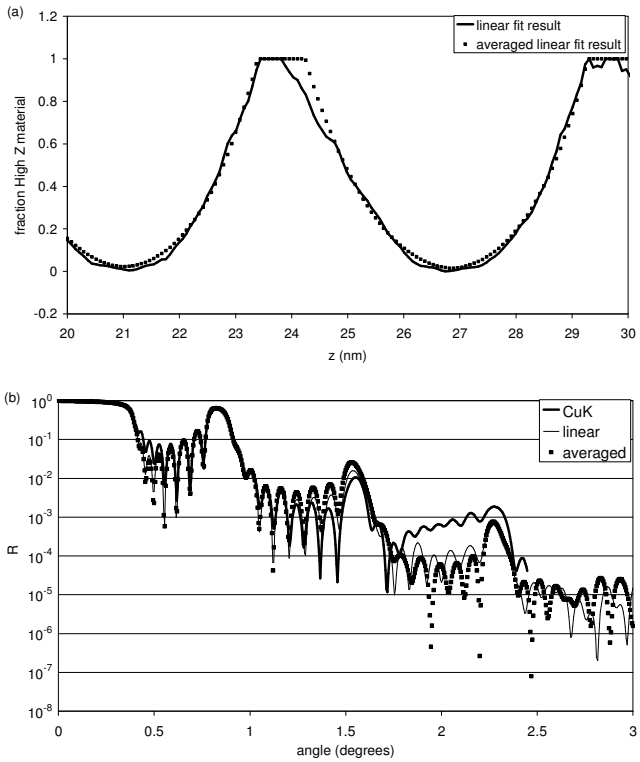

Figure 19a Comparison of the result of the analysis (a) of the W/Si multilayer using the original TEM input profile (solid line) and the 2 nm averaged TEM input profile (dotted line).

Figure 19b Comparison of the calculated reflectivity spectra of the original profile (thin solid line) and the averaged profile (dotted line) to the measured spectrum (thick solid line).

first-order Bragg peak, and the large differences beyond the second order peak. This again confirms our finding that for this method the reflectivity between the critical angle and the first order Bragg peak suffices for analysis, since this range contains the essential data missing in the CS-TEM analysis. The accuracy of the determined profile thus only depends on the resolution of the CS-TEM image.

Typically, the accuracy of the method in determining the d-spacing amounts to less than 1%. Our method is even able to determine the individual interlayer compositions, for example $MoSi_2$ at the Si-on-Mo interface and Mo_3Si_5 at the Mo-on-Si interface. This result is in contrast to the general assumption[6,14,15] that the composition of both types of interlayers is equal. This assumption is based on the limitation of the analysis using reflectometry, which is unable to distinguish a Mo_3Si_5 layer from a thinner $MoSi_2$ layer.[14]

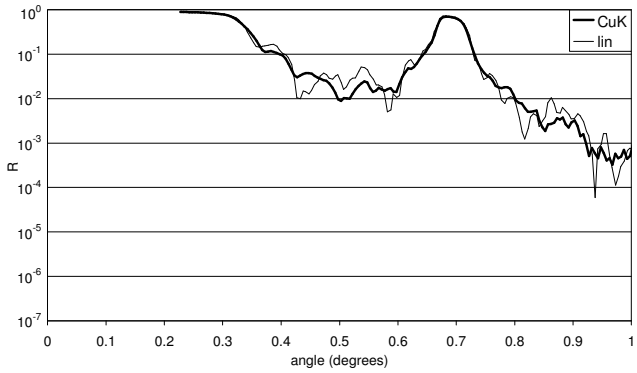

Figure 20 Detail of Figure 18a. Small angle part of measured and fitted reflectivity curves at 0.154 nm (CuKα) of a 50 period Mo/Si multilayer (period thickness 7.2 nm), showing the influence of the wedge-shape of the CS-TEM sample on the calculated reflectivity curve.

The wedged shape of the CS-TEM substrate, as for example seen in the 50 period Mo/Si multilayer structure, has the same effect as a low frequency change in concentration profile. According to the Fourier model this error shows in the reflectometry curves at small angles, and thus at high reflectivities. This part is of considerable influence for the fitting procedure. It is especially important to reduce this wedge error as much as possible for thick structures.. This can clearly be observed in Figure 20, which shows the fitted and calculated reflectivity curves for the 50 period Mo/Si multilayer structure between the critical angle and the first order Bragg peak. Adding an extra parameter, i.e. the wedge angle, in the model used for the fitting procedure might result in an improvement. However, each addition of a free parameter in the fitting routine dramatically increases the risk that the resulting concentration profile does not correspond any more with the real profile.

When we compare the result of the linear fitting routine and the logarithmic fitting routine, especially in the case of the 50-period Mo/Si multilayer mirror, we observed that the logarithmic fit resulted in a better agreement at larger angles and a worse agreement at the smaller angles. However, this logarithmic fit would result in an unrealistic molybdenum silicide structure of which the 13.5 nm near normal incidence reflectivity is largely incorrect (<40% vs. the experimentally measured 61%). We therefore conclude that the logarithmic fitting routine results in an incorrect determination of the density profile.

In order to demonstrate that the results of the analysis are not depending on the use of a-priori information, other than the used materials and the lateral homogeneity, even the most obvious, experimentally determined information was excluded, i.e. oxidation of the

top Si layer. From simulations using software for modelling the optical properties of multilayer films (IMD) written by D. Windt[16] we learned that the effect of oxidation of this layer is primarily observed as changes in reflectivity between the Bragg peaks. This is due to the fact that the optical indices of Si and SiO_2 are very close to each other, as well as very close to the optical index of air. A good fit of the Bragg peaks, as was found in our experimental results, therefore indicates that the determined multilayer structure does agree with the real profile.
An interesting example for demonstrating our method is the standard W/Si multilayer (Figure 14 and Figure 15). Based on the good fit we can assume that the misalignment of the electron beam is negligible and the sample is not prepared in a wedged shape. From the asymmetric density profile (Figure 15c) we therefore can conclude that W diffuses into Si during or after deposition.

3.8 Conclusions

We have developed and demonstrated a method to analyze CS-TEM images, based on a description of the electron-beam absorption in the CS-TEM sample. This enabled us to determine the absolute intensity-to-density-conversion-scale of CS-TEM images by a fit of essentially only three free parameters. Using this result we can obtain a complete quantitative depth-dependent density profile. As input data we only used the refractive indices of the two materials used in the structure, measured x-ray reflectivity data and the CS-TEM image. The single assumption was that the layers of the multilayer structure are laterally homogeneous. It has to be emphasized that no model containing a-priori known information, like compositions, thicknesses and roughnesses of the individual layers and interfaces, was needed to obtain a good agreement with the x-ray reflectometry data used in addition to the CS-TEM. This makes our method more reliable than alternative methods, e.g. standard fits to x-ray reflectivity data.
To achieve sub-nanometer resolution, proper preparation of the CS-TEM sample as well as perfect alignment in the microscope is essential. The experimental results demonstrate that the method can be used to determine the in-depth density profile, thickness, roughness and even stochiometry for each individual layer in the structure.

3.9 Acknowledgments

The authors acknowledge the technical assistance of H. Zeijlemaker and the preparation of CS-TEM samples by T.R. de Kruijff. We are thankful to A. Yakshin for helpful

discussions on the results of the fitting routines and to E. Louis for deposition of the 50-period Mo/Si multilayer mirror. We thank PTB Berlin, Germany for the at-wavelength measurement of this sample.
This work is carried out as part of the research programme of the Stichting voor Fundamenteel Onderzoek der Materie (FOM) with financial support from the Nederlandse Organisatie voor Wetenschappelijk Onderzoek (NWO).

3.10 References

1 E. Spiller, (SPIE (Society of Photo-optical Instrumentation Engineers), 1994).
2 W.W.V.D. Hoogenhof and D.K.G. de-Boer, Materials Science Forum **143-147 pt. 3**, 1331 (1994).
3 P.J.S. Thomas, T.J.C. Hosea, D. Lancefield, and H. Meidia, Semiconductor Science and Technology **16** (2), 107 (2001).
4 M. Tolan, *x-ray scattering from soft-matter thin films*. (Springer-Verlag, Berlin Heidelberg New York, 1999).
5 R.M.A. Azzam and N.M. Bashara, *Ellipsometry and polarized light*. (North Holland Physics publishing, Amsterdam, 1987).
6 A. Aschentrup, W. Hachmann, T. Westerwalbesloh, Y.C. Lim, U. Kleineberg, and U. Heinzmann, Applied Physics a-Materials Science & Processing **77** (5), 607 (2003).
7 L. Reimer, in *Transmission electron microscopy, Physics of image formation and microanalysis* (Springer, 1997), pp. 202.
8 F. Abelés, Annales de Physique **5**, 596 (1950).
9 E.R. Panier and A.L. Tits, Mathematical Programming **59** (2), 261 (1993).
10 C. Lawrence, J.L. Zhou, and A.L. Tits, (1997).
11 This thesis: chapter 5, M.J.H. Kessels, J. Verhoeven, A.E. Yakshin, F.D. Tichelaar, and F. Bijkerk, Nucl. Instrum. Meth. B **222** (3-4), 484 (2004).
12 R. Schlatmann, A. Keppel, S. Bultman, T. Weber, and J. Verhoeven, Appl. Phys. Lett. **68** (21), 2948 (1996).
13 S.P. Murarka, *SILICIDES FOR VLSI APPLICATIONS*. (Academic Press, Orlando, 1983).
14 A.E. Yakshin, E. Louis, P.C. Görts, E.L.G. Maas, and F. Bijkerk, Physica B **283** (1-3), 143 (2000).
15 M.H. Modi, G.S. Lodha, M. Nayak, A.K. Sinha, and R.V. Nandedkar, Physica B **325** (1-4), 272 (2003).
16 D.L. Windt, Comput. Phys. **12** (4), 360 (1998).

4 Ion-induced interface layer formation in W/Si and WRe/Si multilayers

4.1 Abstract

The effects of ion-polishing of the metal layers in W/Si and WRe/Si soft x-ray multilayer mirrors has been investigated, essentially distinguishing between effects at the layer directly being treated by the ions, and at the interface underneath this layer in the stack. Planar transmission electron microscopy (TEM) and calibrated cross-sectional TEM showed counterbalancing effects, in the case of W/Si systems leading to an optimal soft x-ray reflectivity at 100 eV ion energy.

4.2 Introduction

For high quality multilayer mirrors, as for example used in EUV lithography[1] and x-ray microscopy,[2] it is mandatory that the layer quality approaches the ideal Bragg structure. This primarily involves that the individual layers are closed and that the interfaces between the layers are not intermixed and atomically sharp. The latter requirement is also essential for the use of these structures as dispersive elements,[3] as for example in x-ray fluorescence analysis.[4] Several approaches are possible to achieve this goal. Firstly, a good selection of the two multilayer materials is essential, based on both optical and mechanical properties.[5] Secondly, the quality of the layers can be improved by adding energy during or after growth of each individual layer, for example by means of energetic ions.[6,7] This can smoothen the layer surface, resulting in a sharper interface. In case the structures are created using e-beam evaporation, these ions can be applied at any phase of the deposition process e.g. using a Kaufman ion source. In other deposition techniques,

like magnetron or RF sputtering, ions with a broader energy range are present during the entire process. E-beam based deposition, including the use of ions at adjustable energy and from an independent (ion) source, is therefore considered more suitable to study the different ion-surface interaction processes.
However, care has to be taken to prevent a reduction of the quality of the interface(s) *underneath* the layer treated with ions, e.g. by intermixing at these interfaces or the formation of crystallites.[8,9] So far, no specific information is available on the degrading effects of ion bombardment to the layers deeper in the multilayer stack, mainly due to the absence of diagnostics that allows a discrimination of effects at the top and the deeper situated interfaces.
In this paper we have employed a recently developed method[10] to explore the effects at the top and the deeper interfaces of two relevant multilayer combinations, namely W/Si and WRe/Si. The first has been selected for its frequent use in x-ray fluorescence analysis, while WRe/Si was chosen to explore the material dependence after indications of a smoother layer growth of WRe as compared to W.[11,12]

4.3 Experimental

In the fabrication of the W/Si and WRe/Si structures, the ion energy was varied during or after deposition of the W or the WRe layer. For this, we used an e-beam evaporation setup in an ultra high vacuum system (base pressure 1 x 10^{-9} mbar). The WRe mixture contained 70% W and 30% Re. In earlier experiments it was determined that this composition grows in an amorphous[11] and smooth structure.[12] The deposition rate of all materials was approximately 0.01 nm/s. Interference of reflected carbon-K radiation was used to control the film thickness in real time during deposition and during ion treatment.[5] The grazing angle of incidence of the carbon line radiation was 35˚, resulting in a d-spacing of 4.2 nm. A Kaufman ion source (grazing angle of 45˚) was used for treatments of the layers with Kr ions during or after deposition of the individual layers. We varied the energy per deposited atom by changing the ion energy. The selected ion energies (several values in the 0-300 eV range) appeared to have a linear correlation (coefficient of determination equal to 0.98) with the energy per deposited atom (0-65 eV). These energies, which are relatively high compared to chemical formation energies (~1 eV), were found to be necessary due to the very fast relaxation (~10^{-12} s) of the ion-deposited atom system.
Planar bright field TEM was used to determine the lateral growth of the W and WRe layers. The NaCl crystalline substrates needed for this were simultaneously coated with the regular Si substrates in the deposition system. This enabled an accurate control of the deposition process using in situ reflectometry on the Si substrate. The deposited structure

was separated from the NaCl crystal by dissolving the substrate in water, and transferred to a copper grid, to enable planar TEM analysis.

To determine the in-depth structure of the interfaces in the structures, we used cross sectional TEM analysis, for which the intensity-to-density scale was calibrated using x-ray reflectivity measurements.[10] This enabled us to determine the in-depth profile on a *quantitative* scale. The TEM specimen were prepared by sawing and mechanical polishing to ~ 20 µm thickness, followed by ion milling to 50-100 nm (Gatan PIPS model 691). The edge-on position in the TEM was found using the substrate orientation. The TEM photographs were digitized at a resolution of 16 pixels per nm (Nikon super coolscan 8000 ED film scanner). The reflectivity of the sample was characterized prior to TEM preparation by $\theta/2\theta$ reflectometry at CuKα wavelength (0.154 nm) using a Philips X'pert reflectometer.

4.4 W/Si multilayer

4.4.1 Lateral structure

The lateral structure of the deposited W layer was studied using Si/W/Si tri-layer samples made by simultaneous deposition on Si and NaCl substrates. The NaCl based samples consisted of a base layer of 15 nm Si, which was smoothened after deposition by 300 eV Kr^+ ions. A W layer of 1.7 nm was then deposited assisted by bombardment of Kr^+ ions with a total energy ranging from 65 to 200 eV. Combining estimates on ion energy and flux, the impacting kinetic energy per atom deposited was calculated and ranged from 1 to 65 eV. In addition, one sample was produced without Kr bombardment. Finally, one

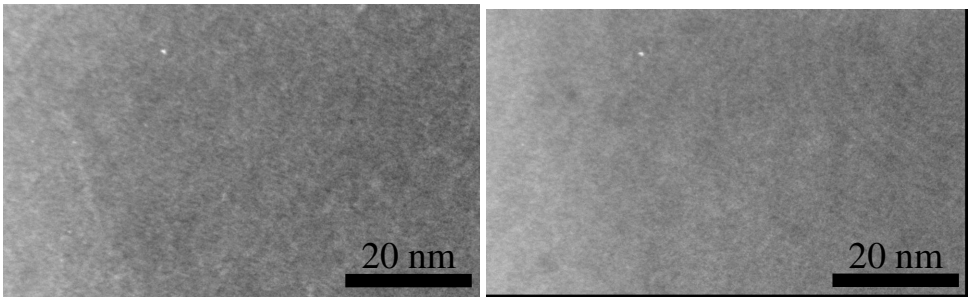

(a) (b)

Figure 21 Planar TEM image of a Si/W/Si tri-layer structure produced without ion treatment (a), and with 300 eV ion treatment of the W layer after deposition (b).

sample was produced using ions (at 300 eV) after deposition of an excess amount of 0.5 nm W, resulting in removal of this excess layer. Finally, the structures were coated with a 4.1 nm thick Si layer to prevent atmospheric influences.
For all ion energies the bright field planar TEM pictures showed a laterally homogeneous structure. Figure 21 shows bright field-TEM micrographs of the sample produced without ion treatment (a) and the sample treated with 300 eV ions after W deposition (b). Ion treatment during deposition at energies between 65 and 200 V resulted in identical images. The absence of any structure in these images indicates that W forms a closed layer on top of Si, independent of the ion treatment or the ion-energy applied.

4.4.2 In-depth structure

In order to measure the interface widths in the structure as a function of the ion energy, we prepared a special multilayer stack with 5 sub-stacks of 3 periods each. Each sub-stack was treated with a different ion energy during or after deposition of W. The Si layers in all sub-stacks were smoothened using 300 eV Kr^+ ions. The W layers in the first sub-stack were smoothened using 300 eV Kr^+ ions after deposition. The W layers in the second sub-stack were grown while assisted by 200 eV ion bombardment. The third sub-stack was made using 150 eV, and the fourth sub-stack using 100 eV. The last sub-stack was deposited without ion treatment of the W layers. By selecting this decreasing ion energy for each sub-stack, the risk of interference of the processes on each of the sub-stacks was reduced, while the choice for combining the sub-stacks into a single multilayer reduced uncertainties from run-to-run deposition instabilities. This multilayer was then characterized using cross-sectional TEM, which was calibrated using CuKα reflectometry. As a result a quantitative density profile was obtained. From this profile we determined that no pure W was observed in those periods in which the W was treated with 300 eV ions after W deposition, since all material was intermixed in these layers. Using this profile we could determine the interface widths. In simulations of multilayer mirrors it is common to describe the density profile $\rho(z)$ at an interface using an error function:[13]

$$\rho(z) = \frac{1}{\sqrt{\pi}} \int_{-\infty}^{z} e^{-t^2/2\sigma^2} \mathrm{d}t \qquad (41)$$

The width of such an interface is then described using the parameter σ, which is equal to the distance between points having concentrations of 16% and 84%.
Using these concentration levels we determined the widths of the interfaces of Si-on-W as well as W-on-Si as a function of energy as shown in Figure 22. To indicate the main trends, a linear fit is drawn (the measurement at 300 eV is not included, see above).

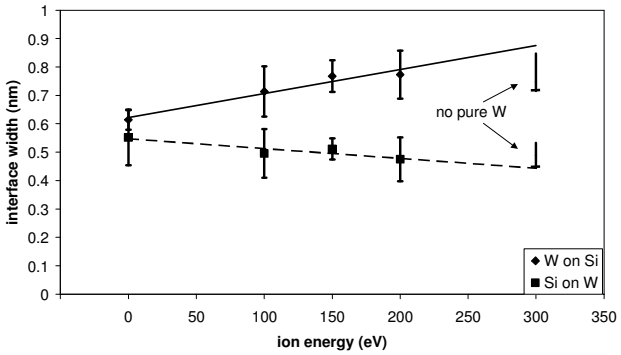

Figure 22 Interface widths of the Si-on-W interfaces (■), and the W-on-Si interfaces (♦) below, plotted as a function of the ion energy applied during or after the W deposition. Indicated are the lower limits of the widths of samples produced at 300 eV.

Figure 22 clearly shows that for increasing ion energy, the interface width of the Si-on-W interface decreases, while the opposite effect is taking place at the W-on-Si interface.

4.4.3 Reflectivity

A third indication of interface properties is obtained from analysis of the in-situ reflectivity during the deposition process. The reflectivity measured at the end of the deposition and ion treatment of the W layer (represented by a maximum positive interference) is plotted as a function of the ion energy in Figure 23 (indicated by ♦-signs and a solid line). An initial improvement in reflectivity can be observed up to an ion energy of approximately 100 eV, while a slow reduction is observed for higher energies. The size of the error bars for the tri-layer systems is determined by noise and alignment uncertainty of the substrates.
This optimal value is also observed for the reflectivity measured after the tenth period in similarly produced 10-period multilayers, as is shown in the same figure (by the ■-signs and the dashed line). These samples were produced with a period thickness of 4.1 nm, consisting of 1.7 nm W and 2.4 nm Si. For these structures the errors are primarily determined by layer thickness variations. The empirically determined errors correspond to an average value of these deviations of approximately 0.2 nm.

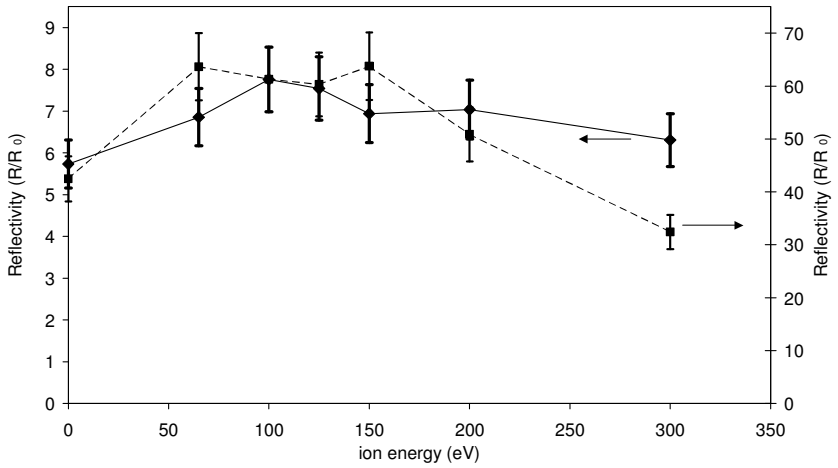

Figure 23 Peak in-situ reflectivity as a function of ion energy applied during the deposition of W in Si/W/Si tri-layers (♦ and solid line) and 10-period stacks (■ and dashed line). The values at 300 eV are obtained using ion treatment *after* deposition of the W layer.

4.4.4 Discussion

The behavior of the reflectivity as a function of ion energy, as observed in Figure 23, cannot be explained by a change in the lateral structure of the W layer, e.g. by island formation, since the planar TEM measurements (Figure 21) revealed no change. In general, the reflectivity decreases when the width of the interfaces increases, e.g. due to interface roughness or partial layer intermixing. Based on the decreasing width of the Si-on-W interface for increasing ion energy, as shown by the dashed curve of Figure 22, we expect an increase in reflectivity. However, this effect is counterbalanced by the increasing W-on-Si interface width.

To explain the presence of a maximum in reflectivity (Figure 23), it is assumed that the reduction of the Si-on-W interface width should initially have more influence on the reflectivity than the increase of the W-on-Si interface. This can be explained when the W-on-Si interface would initially have a very low interface width. This is evident from the Debye-Waller factor, i.e. the reflectivity R of a structure with interfaces having a width σ divided by the reflectivity R_0 of the structure with perfect interfaces:[5]

$$\frac{R}{R_0} = e^{-q_z^2\sigma^2} \quad , \qquad (42)$$

where the wave factor q_z is defined as:

$$q_z = 2\frac{2\pi}{\lambda}\sin\alpha_i \quad , \qquad (43)$$

with α_i equaling the grazing angle of incidence and λ the wavelength of the incident radiation. From Eq. (42), it is evident that very small interface widths have hardly any influence on the reflectivity, but for higher values the influence becomes indeed more prominent.

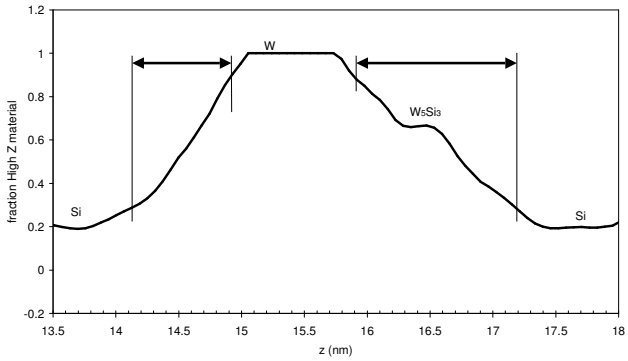

Figure 24 In depth density profile determined from cross section TEM and CuK analysis. Shown is the eleventh period of a 15-period stack. The W layer in this period was treated with 100 eV Kr^+ ions during deposition. Indicated are the interface widths as determined by the 16-84% density levels. The compound at the interlayer is tentatively indicated.

The initially relatively large W-on-Si interface widths determined should thus immediately result in a reduction of the reflectivity for increasing ion energy, which is in contrast to the measured reflectivity. However, the density profile (Figure 24) showed that the W-on-Si interface did not contain one distinct optical interface, but rather two interfaces separated by a compound layer (Si_3W_5, small plateau in Figure 24). Therefore, our interface width as determined by the error function is too large. If we use the true, split, W-on-Si interface widths, with reduced initial values, we can now explain the initial improvement of the reflectivity and thus the occurrence of a global maximum.

To explain the cause of the increased W-on-Si interface widths in some more detail, we calculated the energy transferred from the krypton ions to the W atoms as function of the ion energy and depth. The computer program SRIM[14] was used for that purpose, which calculates the implantation depth and energy transfer of ions in matter. In Figure 25 we show the penetration depth of ions at which, on average, at least 1 eV energy is transferred to the W atoms for different initial ion energies. From this graph it is evident that, taking into consideration the small chemical binding energies (~1 eV) and the thickness of the W

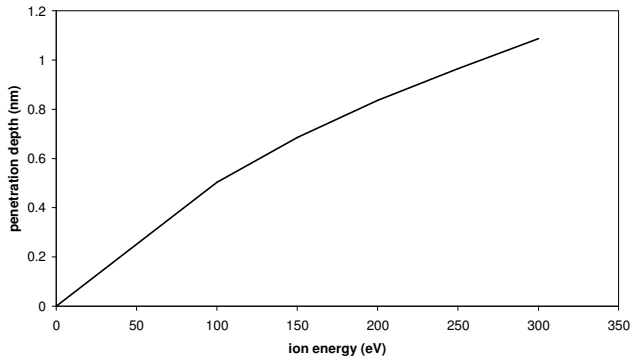

Figure 25 Calculated penetration depth of ions transferring at least 1 eV energy to the W atoms as function of the initial ion energies between 100 and 300 V.

layer, which is at most 2 nm, and much thinner when ions are applied during the growth, ions inevitably reach the interface between the W layer and the Si layer underneath, and will cause intermixing of the W and Si in the next interface in the multilayer structure.[15]
A global picture of the growth of the W/Si structure as a function of the ion energy based on these results is illustrated in Figure 26. Both the reduced roughness on the W layer surface as the increasing intermixing at the W-on-Si interface (indicated using diagonal black lines) is shown. At 300 V ion energy the W layer is fully intermixed with Si.

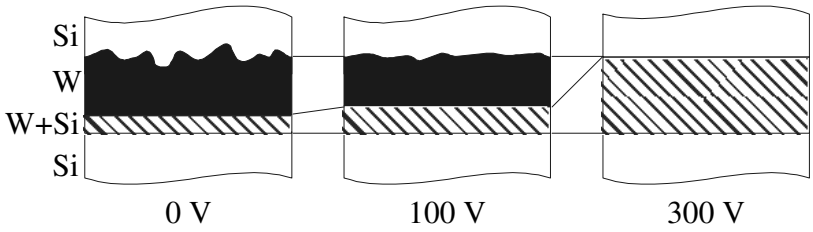

Figure 26 Visualization of expected in-depth density distribution for one period of W/Si

4.5 WRe/Si multilayers

4.5.1 Lateral structure

Analogously to the experiments on the W/Si combination, we analyzed the planar WRe structure in Si/WRe/Si tri-layers. W and Re have nearly the same, high, absorption coefficient and will therefore appear as the dark parts in the TEM image. Figure 27 shows

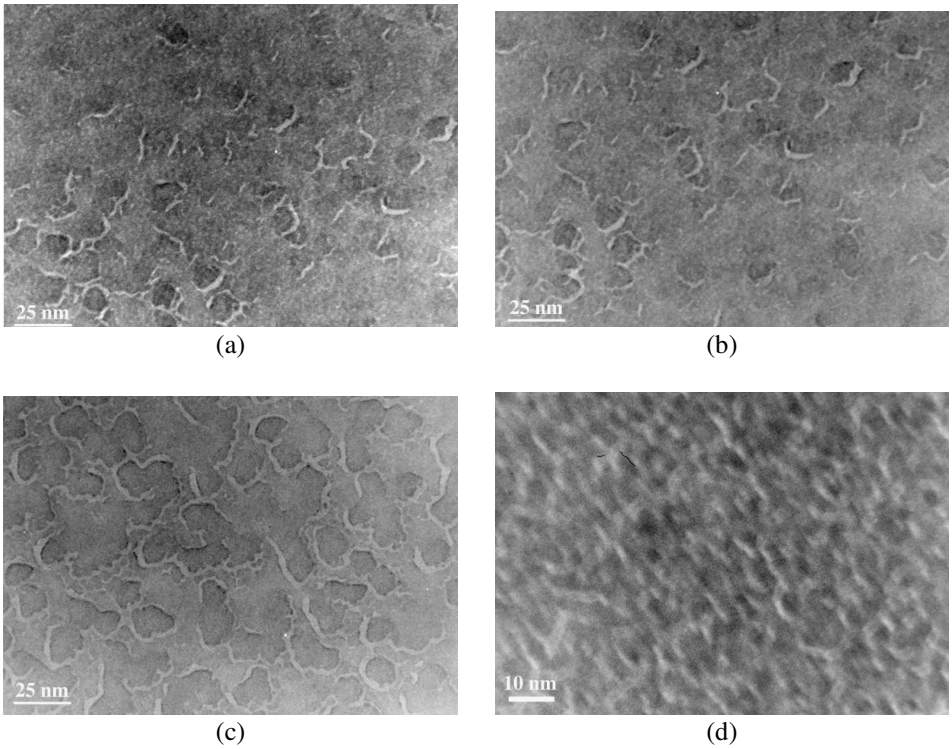

(a) (b)

(c) (d)

Figure 27 Planar TEM image of Si/WRe/Si structures produced without ion treatment of the WRe layer. The thickness of the WRe layer was 1 nm (a), 2 nm (b), 3nm (c), 6nm (d). The image at 6 nm is blurred due to thermal drift of the sample.

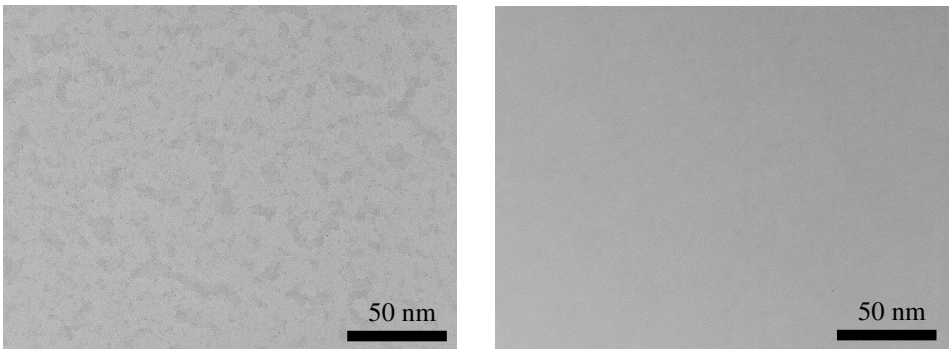

(a) (b)

Figure 28 Planar TEM image of Si/WRe/Si structures produced using ion treatment of the WRe layer. The ion energy was 65 eV (a) and 100 eV (b).

that the WRe layers deposited without ion bombardment are not closed. Increasing the thickness of the WRe layer up to 6 nm did not result in larger island structures nor a higher degree of coverage of the layer (Figure 27b, c, and d). When ion bombardment is applied during deposition, the lateral homogeneity of the WRe layer appears to improve at an ion energy of 65 eV as is visible from the almost abundant lateral structure in Figure 28a, while 100 eV ions result in a laterally homogeneous layer (Figure 28b). No additional change is observed when the ion energy is increased even further.

4.5.2 In-depth structure

In order to determine the change in roughness of the WRe/Si structures, we measured rocking curves using Cukα radiation. Qualitative analysis of these data showed that the roughness of the Si-on-WRe interface is reduced when ion-assisted deposition is applied. We did not perform the cross-sectional TEM analysis here because the island-like structure will be seen as intermixing due to the lateral, 2D averaging inherent to TEM analysis.

4.5.3 Reflectivity

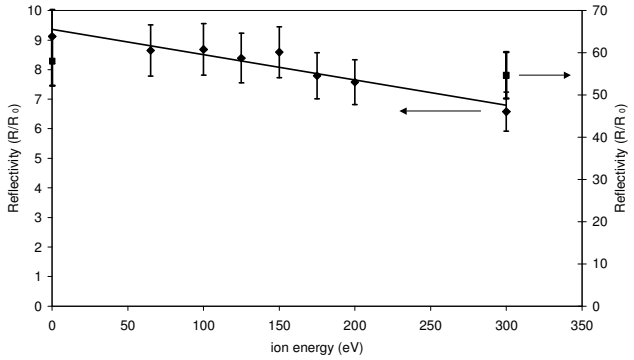

Figure 29 Peak in-situ reflectivity as a function of ion energy applied during the deposition of WRe in Si/WRe/Si sandwiches (♦ and solid line, left axis) and 10 period WRe/Si structures (■ and right axis). The value at 300 eV is obtained using ion treatment after deposition of the WRe layer. A continuous decrease of the reflectivity is observed for increasing ion energy.

We also recorded the peak reflectivity during the growth of Si/WRe/Si structures (Figure 29, indicated by ♦-signs, measurement at 300 eV resulting from ion beam smoothening *after* deposition of the WRe layer). A monotonous decrease of the reflectivity is observed for increasing ion energy. The same trend, although less pronounced, is also observed in the reflectivity dependence of similarly produced 10-period multilayers (indicated by ■-

signs). In view of the monotonous behavior of the reflectivity of the single WRe layers, only samples at the two extreme values of the ion energy were produced (0 and 300 eV).

4.5.4 Discussion

In contrast to the W/Si samples, clear island formation is observed in the planar TEM images of the Si/WRe/Si structures. A negative effect on the reflectivity is expected from the voids between the islands (no reflection) and the edges of the islands (off specular scattering of the radiation). However, the reflectivity of the 10-period WRe/Si multilayer is even higher than the best reflecting W/Si multilayer. Since the island structure is present in all untreated samples, it must be concluded that W and Re have a higher affinity to each other than to Si, as well as to themselves. This would namely result in lower diffusion of WRe into Si and sharper interfaces as compared to the W/Si interfaces. However, this tentative explanation is not supported by the large chemical and physical similarity of W and Re, obviously requiring further investigation, e.g. by STM analysis.
Another unexpected difference between WRe/Si and W/Si is the continuous decrease of the reflectivity of the WRe/Si sample for increasing ion energy. This implies that no, or almost no reduction of the Si-on-WRe interface widths occurs, i.e. in line with the diffuse scattering measurements, so that the increased diffusion at the WRe-on-Si interface is likely to be the dominant effect.
According to specular reflection theory, an intermixed interface does not cause any off-specular scattering of radiation, so the diffuse scattering measurements show only the effect of roughness, mainly caused by the island formation. This indeed decreases as the ion energy is increased, which is in agreement with the disappearance of the islands, as observed in the planar TEM images. A summary of the effects of the ions on the WRe/Si structure is illustrated in Figure 30. Without the use of ions, flat WRe islands are formed on top of Si. Using ions at increasing energies, the islands disappear, and intermixing of the WRe with the Si underneath occurs (indicated by diagonal lines). At an ion energy of 300 V no pure WRe will be present, indicated as a complete mixture of WRe and Si, similar the W/Si case. This is revealed by the similar reflectivity of the 1-period W/Si and WRe/Si structures.

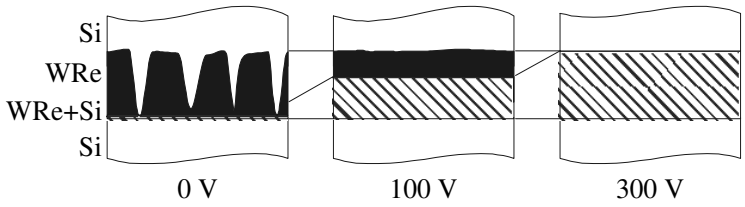

Figure 30 Visualization of expected in-depth density distribution for one period of WRe/Si

4.6 Conclusions

We have investigated the influence of ion bombardment on the layer and the interface structure of W/Si and WRe/Si multilayers, thereby essentially distinguishing between ion-induced effects occurring at the top layer and the layer underneath. We conclude that the ion treatment of W reduces the roughness of the W surfaces, but simultaneously increases the intermixing at the W-on-Si interfaces underneath the directly treated layer, notably by diffusion and compound formation. An optimal value of the ion energy of 100 eV has been determined leading to an improvement of the soft x-ray reflectivity.
Without ion-treatment, WRe was found to form sharp interfaces with Si, resulting in a higher reflectivity of the corresponding WRe/Si multilayer structures as compared to both treated and untreated W/Si multilayers. Although the WRe layer was found to be smooth, it is not closed at the 1 to 6 nm thickness here applied. Ion treatment of this layer resulted in the formation of a closed layer, but intermixing of WRe with the Si layer underneath caused an overall reduction of the reflectivity.

4.7 Acknowledgments

The authors acknowledge the technical assistance of H. Zeijlemaker and are grateful to T.R. de Kruijff for preparation of the cross sectional TEM samples.
This work is carried out as part of the research programme of the Stichting voor Fundamenteel Onderzoek der Materie (FOM) with financial support from the Nederlandse Organisatie voor Wetenschappelijk Onderzoek (NWO).

4.8 References

1 J.E. Bjorkholm, Intel Technology Journal **Q3'98**, 1 (1998).
2 A.G. Michette, Rep. Prog. Phys. **51** (12), 1525 (1988).
3 This thesis: chapter 2, M.J.H. Kessels, J. Verhoeven, and F. Bijkerk, to be published.
4 P.J. Potts, A.T. Ellis, P. Kregsamer, J. Marshall, C. Streli, M. West, and P. Wobrauschek, J. Anal. At. Spectrom. **19**, 1397 (2004).
5 E. Spiller, (SPIE (Society of Photo-optical Instrumentation Engineers), 1994).
6 E.J. Puik, M.J. van der Wiel, H. Zeijlemaker, and J. Verhoeven, Appl. Surf. Sc. **47**, 251 (1991).

[7] E.J. Puik, M.J. van der Wiel, H. Zeijlemaker, and J. Verhoeven, Thin Solid Films **193/194**, 782 (1990).

[8] F. Eriksson, G.A. Johansson, H.M. Hertz, and J. Birch, Opt. Eng. **41** (11), 2903 (2002).

[9] R.W.E. van de Kruijs, E. Louis, A.E. Yakshin, E. Zoethout, I.J.W. Wever, F. Bijkerk, J. Verhoeven, R. Delhez, J.-D. Kamminga, J. Trenkler, S. Müllender, T. Bigault, and E. Ziegler, presented at the 6th International Conference on the Physics of X-Ray Multilayer Structures, Chamonix, France, 2002 (unpublished).

[10] This thesis: chapter 3, M.J.H. Kessels, F.D. Tichelaar, J. Verhoeven, and F. Bijkerk, submitted.

[11] A.W.D.v.d. Gon, J.C. Barbour, R.d. Reus, and F.W. Saris, J. Appl. Phys. **61** (3), 1212 (1987).

[12] R.-P. Haelbich, A. Segmuller, and E. Spiller, Appl. Phys. Lett. **34** (3), 184 (1979).

[13] D.L. Windt, Comput. Phys. **12** (4), 360 (1998).

[14] J.F. Ziegler, SRIM the stopping and range of ions in matter (Annapolis, 2000).

[15] This thesis: chapter 5, M.J.H. Kessels, J. Verhoeven, A.E. Yakshin, F.D. Tichelaar, and F. Bijkerk, Nucl. Instrum. Meth. B **222** (3-4), 484 (2004).

5 Ion beam induced intermixing of interface structures in W/Si multilayers

5.1 Abstract

The impact of energetic ions during fabrication of W/Si multilayers may result in interface layers with a gradually changing concentration, notably in the W-on-Si interface layer. This process may be employed to deliberately form a multilayer system with a graded refractive index within each period, in principle allowing an adjustment of the optical, wavelength-selective properties of the multilayer system. We also have given a first demonstration of a new method based on a combination of high-resolution TEM image analysis and grazing incidence x-ray reflectivity analysis to determine the in-depth density profile of a multilayer structure.

5.2 Introduction

X-ray reflecting multilayer mirrors can be synthesized for a broad wavelength band in the soft x-ray to XUV range (~0.1 to ~30 nm). The reflected intensity as well as the bandwidth, or selectivity, of such a multilayer mirror scales with the number of individual layer interfaces contributing to the reflection process. Selectivity is of relevance for e.g. the use of multilayer systems as monochromators in x-ray fluorescence analysis.[1] Any deviation of perfectly sharp interfaces causes a decrease of the theoretical reflected intensity. However, Fraerman et al.[2] showed that by intermixing the multilayer components at one or both of the interfaces, the selectivity could be increased, though at the expense of the reflectivity. In this paper we investigated this principle in more detail,

where we use the density gradient of the intermixed interface as an additional parameter in the process of optimizing the multilayer selective properties.*

In general, intermixing is caused by chemical interaction of the components. However, also energetic particles, i.e. ions and neutrals, arriving at the substrate during the deposition process, can cause considerable intermixing effects at the interfaces of the layers grown. Especially in sputter deposition of thin films, the layers grown are exposed to particles with energies in the keV range.[3] Using e-beam evaporation, the application of energetic ions with energies of 100eV and higher during or after deposition of the single layers of a multilayer structure has been demonstrated to result in a smooth surface of the deposited layer.[4] A disadvantage of deposition using ions with moderate to high energies is that damage can be caused at the interface underneath.

The effect of ion beam enhanced intermixing depends not only on the material components involved, but also on the order of deposition of the materials. Verhoeven et al.[5] demonstrated that an interface of Si on Mo is less affected by intermixing from energetic ion impact than an interface of Mo on Si. Schlatmann et al.[6] investigated the effect of energetic ions on intermixing of Mo on Si. They found that intermixing of the Mo on Si interface resulted in the formation of an interlayer with a uniform composition of Mo_5Si_3. The thickness of these Mo_5Si_3 layers corresponded to the penetration depth of the ions during intermixing. It has been found that these interlayers are formed even without any energetic ion interaction, and that silicides are always present at each of the two types of interfaces (Mo-on-Si and Si-on-Mo).[7] However, as long as all interfaces of these interlayers are sharp, a proper layer thickness distribution within each period of the multilayer can be found so that the reflectivity does not deviate too much from the theoretical reflectivity of a system with pure Si and Mo. Although several demonstrations of near-theoretical reflectivities of up to 69.5% at normal incidence of 13.5 nm radiation have been given, some demanding applications of multilayer systems, such as extreme ultraviolet lithography, do necessitate specially synthesized interface layers to increase the reflectivity.[8]

For these applications, as well as for other material combinations, it is necessary to further investigate the effect of ions on the interface formation in more detail. In this paper, we report on experiments with the material combination tungsten and silicon, commonly used in multilayer mirrors in the wavelength range of 1 to 5 nm. These experiments revealed

* This chapter was written before the theoretical study described in chapter 2 of this thesis was performed. In retrospect, the argument to perform this investigation to improve the selectivity of such a structure is therefore no longer valid. Nevertheless, graded index structures can be applied in other applications, like anti-reflection coatings or as waveguides.

that W on Si appeared to be less stable than Si on W. There was also a strong indication that an interlayer with a graded composition was formed. We studied the formation of these interlayers, caused by ion bombardment, and especially the in depth density profile. Therefore we followed the approach of Schlatmann[9] and removed the total overlayer of W on Si and investigated the multilayer that was formed.

X-ray reflectometry as well as TEM were used to investigate the in depth profile of the interlayer. In order to be able to quantify the layer profile, we have applied a novel analysis method in which cross sectional TEM has been combined with x-ray reflectometry in such a way that both techniques complements each other. Both TEM and reflectometry are, when used separately, either insufficient accurate or lack the information to determine the actual in-depth density profile: reflectometry is limited because only a part of the reflected amplitude spectrum is measured, while the phase spectrum is not measured at all (an undetermined phase spectrum results in an infinite number of solutions for the density profiles, albeit that many of them are physically not possible[10]). In case the profile is already well known (e.g. layer thicknesses, interface thicknesses, interface profile, etc.), and thus the number of free parameters is reduced, one can find the missing data using a fit of the reflectivity curve with programs like IMD.[11] This program, which calculates the specular reflectivity for a given multilayer structure, provides the possibility to mimic the interface profile by using different predefined functions (error-function, exponential, linear or sinusoidal). However, it is not possible to calculate the optical properties for an arbitrary density profile.

On the other side, cross section TEM is limited for determining the density profile, because an absolute scale for the measured image intensities, and therefore the materials density, is missing. The image intensity is determined by many unknown parameters, like the thickness of the sample, the absorption coefficients of the materials, exposure times, development times of the film and many other factors. Moreover, by changing the focus of the microscope, edges in the image can be enhanced or suppressed. Our new method will overcome the deficiencies of the two separate analysis techniques.*

* The method described in this chapter to calibrate the TEM intensity profiles using reflectometry measurements, has been superseded by the method described in chapter 3 of this thesis. However, the results and conclusions obtained here are not affected by the choice of the method.

5.3 Experimental

We used e-beam evaporation in an ultra high vacuum system (5 x 10^{-8} mbar) to deposit W/Si multilayer systems on Si (100) substrates. Interference of reflected carbon-K radiation was used to control the film thickness in real time during deposition and during ion treatment.[12] The grazing angle of incidence of the carbon line was 35° resulting in a multilayer structure with a periodicity of 4 nm. A Kaufman ion source (grazing angle of 45°) was applied for different treatments of the layers, including layer intermixing. In order to be able to relate our results on W to the earlier results of Schlatmann[9] on the Mo/Si system, we used a higher energy for the Kr ions. From TRIM simulations an energy of 1000 eV was determined for the W/Si system, as opposed to 300 eV for the Mo/Si system, to maintain a constant ion energy-mass ratio during the ion bombardment.[13]

We characterized the multilayers by θ:2θ reflectometry using an x-ray reflectometer at Cu-Kα wavelength (Philips MRD). Cross sectional TEM (Philips CM30T, 300 keV) was used to further investigate the multilayer structure. TEM cross sectional specimens were prepared by sawing and mechanical polishing to ~ 20 µm thickness, followed by ion milling (Gatan PIPS model 691). Putting the specimen in the edge-on position in the TEM was done with the help of the substrate orientation. A small deviation of the substrate surface from the (100) orientation of about 3° was taken into account when positioning the multilayer sample.

As argued before, cross sectional TEM and reflectometry are combined in order to determine the in-depth density profile. First, we scan the TEM pictures and form an intensity profile. Next, we average over all periods available and over a lateral scale of about 10 nm. This statistically improves the data. Since the attenuation factor for electrons in silicon is approximately ten times smaller than the attenuation factor in tungsten[14] we can neglect the absorption of electrons by silicon. Though in the present setup this boundary condition limits the use of this method, it is generally fulfilled for soft x-ray mirrors. Thus the transmission of the electrons T depends exponentially on the concentration of high density material (tungsten) (C_W):[14]

$$T = e^{-kC_W}, \qquad (44)$$

where k is a constant depending on thickness of the sample and the absorption of tungsten. When we additionally assume that the TEM film and scanner is operated within the linear range, the measured intensity I depends on the transmission T according:

$$I = aT + b, \qquad (45)$$

where *a* and *b* are related to the optical properties of the imaging system (e.g. brightness or contrast). This results in a dependency of the measured intensity on the concentration of tungsten according to:

$$C_W = -\frac{\ln\left(\frac{I-b}{a}\right)}{k}. \qquad (46)$$

If we now assume that the maximum intensity I_{max} measured corresponds to 0% tungsten and the minimum intensity I_{min} corresponds with 100% tungsten, we may put *a* equal to I_{max}-*b* and *k* equal to -ln((I_{min} –*b*)/ (I_{max} –*b*)), which gives:

$$C_W = \frac{\ln\left(\frac{I-b}{I_{\max}-b}\right)}{\ln\left(\frac{I_{\min}-b}{I_{\max}-b}\right)}. \qquad (47)$$

Equation (47) contains only *one* free parameter (*b*), which is to be determined by a fit to experimental data.

By varying the parameter *b* we can fit the calculated spectra based on the concentration profile determined by equation (47) to the measured θ:2θ reflectometry spectrum. This enables us to determine an accurate in-depth density profile of the multilayer structure.

5.4 Results

The in-situ reflectivity curve representing the deposition process is shown in Figure 31. In each period we deposited 5 nm of silicon. This was followed by etching using 300 eV Kr ions, until an interference maximum was reached in the in-situ reflectivity signal, corresponding to a remaining Si layer of 4 nm. The increased reflectivity at this interference maximum indicates a reduction of the surface roughness of the silicon layer[12]. We continued to deposit an overlayer of 1 nm W. This overlayer was then completely removed by Kr ions with an energy of 1000 eV. As a result, W was partly forced into the silicon layer. The ion treatment was stopped again at the interference maximum, corresponding to a 4 nm thick layer of what is later shown to be a mixture of W and Si. We repeated this process 10 times to get a periodic 10-bilayer structure. The total increase of the reflectivity by a factor of 40 observed from the beginning of the deposition, indicated the formation of a good multilayer mirror.

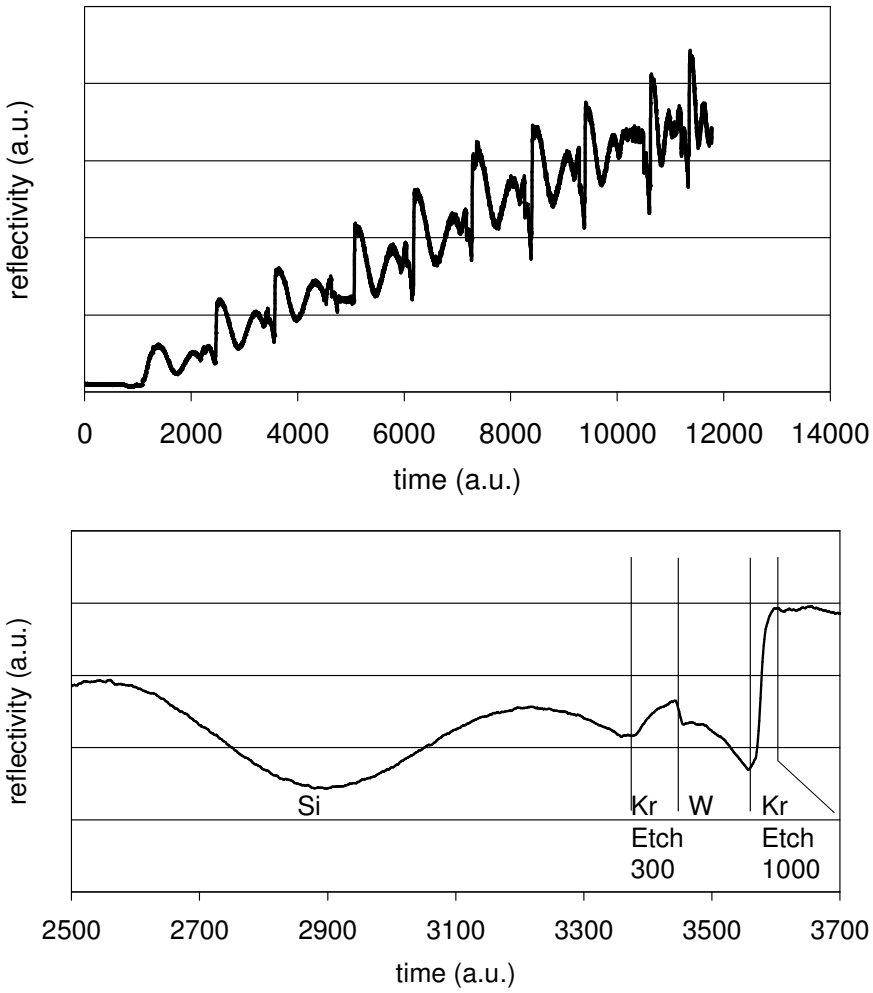

Figure 31 X-ray reflectivity signal indicating the layer thickness during the deposition process. In figure b the production of one period is shown. The four steps (Si deposition, smoothening of Si, W deposition and intermixing) are indicated.

Figure 32a shows the cross sectional TEM picture of the W/Si multilayer on which this deliberate intermixing was applied. For comparison, the cross sectional TEM picture of the intermixed Mo/Si sytem as produced by Schlatmann et al. is shown in Figure 32b,

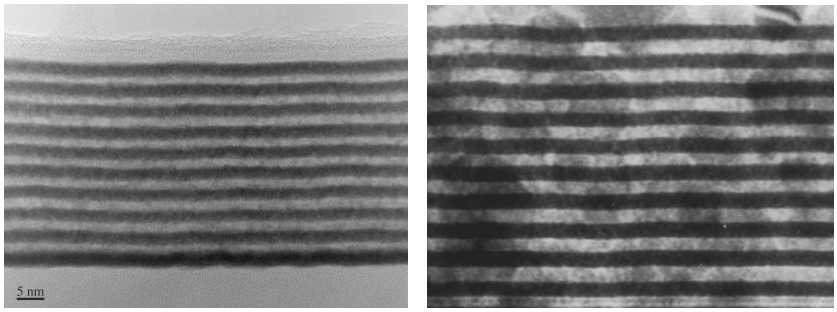

Figure 32a. Cross sectional TEM image of a W/Si graded index multilayer with 4 nm period. The image shows more diffuse interfaces as compared to the interfaces of the Mo/Si sample shown in Figure 32b.

Figure 32b. Result of intermixing experiment by Schlatmann et al. Visible is a very sharp interface between the pure Si layer (light) and the (uniformly) mixed Mo_5Si_3 layer (dark). The period of this multilayer is 6 nm.

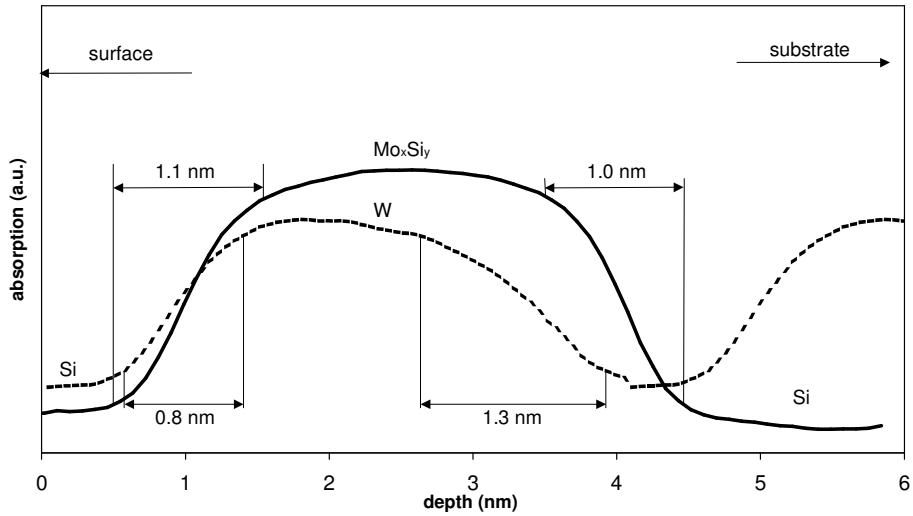

Figure 33 Measured absorption profiles of cross sectional TEM images of W/Si (dashed line) and Mo/Si (solid line) multilayers. The scales are identical. Note the asymmetric profile of W/Si vs the symmetric profile of Mo/Si, the W-on-Si interface showing the graded profile. The interface widths indicated are determined using absorption levels of 10 % above the minimal value and 10% below the maximum value. *A calibrated density profile of this W/Si structure, using the method described in chapter 3, can be found in Figure 16b.*

showing the uniform Mo_5Si_3/Si interface structures with sharp layer boundaries. The images were analyzed, resulting in Figure 33, which shows the normalized intensity profile after averaging over all periods.

By taking the logarithm of the normalized W/Si intensity profile, we obtain a relative density profile of this structure as given by formula (47). This density profile is then used to calculate the θ:2θ reflectometry spectrum of this structure. The result is plotted in Figure 34 (solid line). The measured θ:2θ reflectometry spectrum is represented by the points in Figure 34.

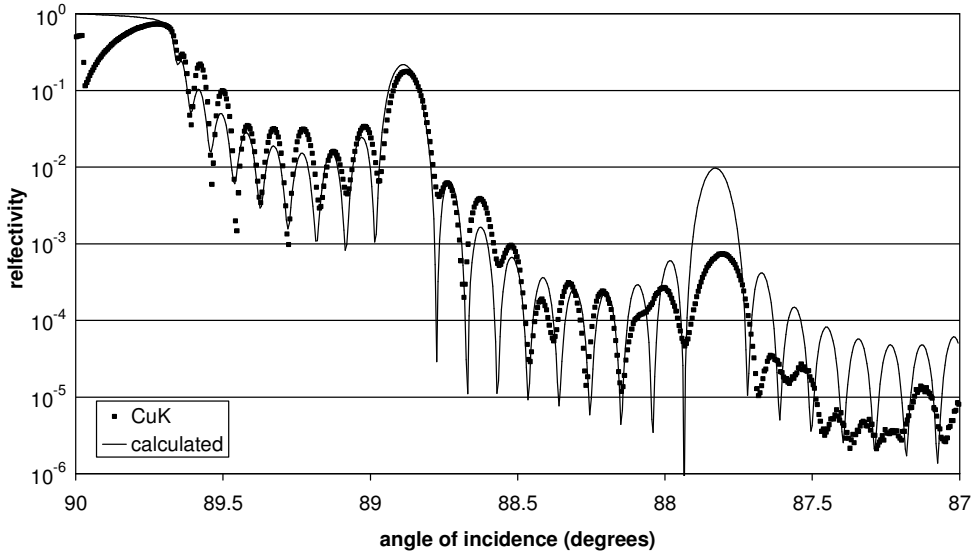

Figure 34 Comparison of measured (points) and calculated (line) reflectivity as a function of angle of incidence. The calculated data is solely based on the intensity measurements of the cross sectional TEM image. The good similarity shows the power of this method.

5.5 Discussion

When comparing the intensity profiles (Figure 33), we see that the profile of the Mo_5Si_3/Si system (solid line) is clearly symmetric, while the profile of the W/Si system (dashed line) is asymmetric. The Si-on-W transition layer has a width of 0.8 nm, similar to both the transition layers of the Mo_5Si_3/Si system. The thickness of the W-on-Si transition layer however, is 1.3 nm, while the density gradient is notably lower. It can also be observed that the total depth of intermixing for the Mo_5Si_3/Si system is ≈ 3.5 nm for using 300 eV

Kr^+ ions while 1 keV Kr^+ ions were required to intermix W to the same depth into Si. This confirms the TRIM result on the adapted Kr^+ energy. These experiments clearly show that the ion beam intermixing process, when applied to W on Si, results in a graded density profile, in contrast to the behaviour of Mo and Si found by Schlatmann et al.[6]

The similarity between the calculated and the measured θ:2θ spectrum demonstrates the accuracy of our analysis of the TEM results. It is noted that in the experimental fitting procedure the value of b was found to be very close to I_{min}, which suggests that the relation given in formula (47) is more general and not dependent on a fitting procedure. However, to determine if this method is generally applicable, further research using different materials and different density profiles is necessary. It should be emphasized that no proper curve fitting could be made using the program IMD[11], since it uses predefined interface profiles, which do not correspond to the experimentally determined profiles.

Using the program TRIM[13] we can, based only on mechanical interaction of ions and matter, indeed simulate a graded profile as found in the TEM analyzed W/Si multilayer. However, when considering mechanical interaction only, i.e. as is done in the TRIM simulation algorithm, ion induced intermixing of Mo into Si would also result in a graded density profile. This discrepancy with the experimental results found by Schlatmann et al. can be explained by considering the chemical interaction between the two multilayer materials. In general, the formation of alloys is a thermodynamical process depending on the free Gibbs energy G. When we know the enthalpy of alloy formation ΔH, the temperature T and the entropy of formation ΔS, the Gibbs free energy can be calculated using:

$$\Delta G = \Delta H - T\Delta S \qquad (48)$$

In Table 2 we listed the values of ΔH and ΔS of all compounds of W or Mo with Si. Since the values of ΔS are much lower than the values of ΔH, we can use ΔH to determine the likelihood of formation of the particular compound.

Compound	ΔH (kJ/(mole of atoms))	ΔS (kJ/(K mole of atoms))
$MoSi_2$	-44	-0.0015
Mo_5Si_3	-39	+0.0001
Mo_3Si	-28	+0.0003
WSi_2	-31	-0.0021
W_5Si_3	-17	+0.0013

Table 2 Formation enthalpies ΔH and the entropy ΔS of the compounds investigated. All values are measured at a temperature of 298 K [15].

From this table we can see that the W rich compound W_5Si_3 has a significantly lower enthalpy of formation than any Mo compound. Also, the Si rich compound WSi_2 has a lower enthalpy of formation than the corresponding Mo compound $MoSi_2$. This means that these tungsten compounds are less likely to be formed and are easier to be dissociated as compared to the corresponding molybdenum compounds. The lower energy released upon formation of W-Si compounds is therefore argued to allow an interface layer with a gradual change of the composition without discontinuities caused by distinct compound formation. It is thus found that ion induced intermixing of Mo into Si requires a thermodynamic correction of the classical mechanical laws describing the intermixing process.

5.6 *Conclusions*

We have shown that impact of energetic ions during fabrication of W/Si multilayers results in a graded density profile, notably of the W-on-Si interface layer. This effect should therefore be taken into account of the multilayer design. Nevertheless, this process may be employed to deliberately form a multilayer system with a graded refractive index within each period, in principle allowing an adjustment of the optical, wavelength-selective properties of the multilayer system. The result is in contrast to the results found by Schlatmann et al. on Mo/Si multilayers showing an intermixed layer of constant composition and sharp interface boundaries. The difference is explained by the chemical stability of the respective compound material formed at the layer interfaces, i.e. its heat of formation as described by classical thermodynamics. We also demonstrated that a combination of high-resolution TEM image analysis and grazing incidence x-ray reflectivity analysis confirms the formation of a graded density profile, and have shown that this is a viable method to investigate in-depth density profiles.

5.7 Acknowledgments

The authors acknowledge the technical assistance of H. Zeijlemaker and the preparation of TEM samples by T. R. de Kruijff.
This work is carried out as part of the research programme of the Stichting voor Fundamenteel Onderzoek der Materie (FOM) with financial support from the Nederlandse Organisatie voor Wetenschappelijk Onderzoek (NWO).

5.8 references

[1] R. Jenkins, in *Encyclopedia in Analytical Chemistry*, edited by R.A. Meyers (John Wiley & Sons Ltd., Chichester, 2000), pp. 13269.

[2] A.A. Fraerman, S.V. Gaponov, V.M. Genkin, and N.N. Salashchenko, Nuclear Instruments and Methods in Physics Research Section A: Accelerators, Spectrometers, Detectors and Associated Equipment **261** (1-2), 91 (1987).

[3] B.N. Chapman, in *Glow discharge processes* (John Wiley & Sons, Inc., 1980), pp. 177.

[4] E.J. Puik, M.J. van der Wiel, H. Zeijlemaker, and J. Verhoeven, Appl. Surf. Sc. **47**, 63 (1991).

[5] J. Verhoeven, L. Chunguang, E.J. Puik, M.J. van der Wiel, and T.P. Huygen, Appl. Surf. Sc. **55**, 97 (1992).

[6] R. Schlatmann, A. Keppel, S. Bultman, T. Weber, and J. Verhoeven, Appl. Phys. Lett. **68** (21), 2948 (1996).

[7] A.E. Yakshin, E. Louis, P.C. Görts, E.L.G. Maas, and F. Bijkerk, Physica B **283** (1-3), 143 (2000).

[8] S. Bajt, J.B. Alameda, T.W. Barbee, W.M. Clift, J.A. Folta, B. Kaufmann, and E.A. Spiller, Opt. Eng. **41** (8), 1797 (2002).

[9] R. Schlatmann, A. Keppel, S. Bultman, and J. Verhoeven, presented at the Meeting on Physics of X-ray Multilayer Structures, Jackson Hole, WY, USA, 1994 (unpublished).

[10] M. Tolan, *x-ray scattering from soft-matter thin films*. (Springer-Verlag, Berlin Heidelberg New York, 1999).

[11] D.L. Windt, Comput. Phys. **12** (4), 360 (1998).

[12] E. Spiller, (SPIE (Society of Photo-optical Instrumentation Engineers), 1994).

[13] J.F. Ziegler, SRIM the stopping and range of ions in matter (Annapolis, 2000).

[14] L. Reimer, in *Transmission electron microscopy, Physics of image formation and microanalysis* (Springer, 1997), pp. 202.

[15] F.R. de Boer, R. Boom, W.C.M. Mattens, A.R. Miedema, and A.K. Niessen, *Cohesion in Metals: Transition metal alloys*. (North-Holland Physics Publishing, Amsterdam, 1988).

6 Si adhesion interlayer effects in hydrogen passivated Si/W soft x-ray multilayer mirrors

6.1 Abstract

The use of hydrogen passivation of the silicon layers in Si/W soft x-ray reflective multilayer mirrors is investigated. Standard passivation, corresponding to Si:H/W structures, led to reduced growth properties of the W layers. The additional use of atomically thin Si adhesion layers, corresponding to Si:H/Si/W, led to improved growth and increased soft x-ray reflectivity. The effects taking place at the interfaces are analysed by bright field planar TEM and in-situ x-ray reflectivity, and are described in terms of interface and surface energies, with quantitatively analysis of intermixing, materials density, and geometrical optical effects.

6.2 Introduction

High reflectivity is of paramount importance for soft x-rays reflective multilayer systems, and is critically dependent on the practical realization of optically sharp interfaces.[1,2] A key task in this is to reduce the atomic interdiffusion of the multilayer materials as well as phenomena such as a non-uniform, island-like growth of the components. These two effects, interdiffusion and non-uniform growth, are largely determined by the chemical and physical properties of the individual materials and their mutual chemical interaction. From previous work[3] it is known that metals like Mo and W diffuse easily into Si: Mo tends to form a compound with Si, whereas W forms a depth dependent mixture with Si.

A common technique to reduce interdiffusion of these material pairs is the use of diffusion barriers[4], composed of a third material selected for its low diffusion into the two main components. This barrier layer should have a certain minimal thickness to allow the blocking of the interdiffusion, but it should also be as thin as possible to reduce the influence on the multilayer optical properties. Multilayer systems for the soft x-ray range (0.1-10 nm) need to have layer thicknesses down to a few atomic layers, which makes the barrier layer concept of limited practical value.

The more pragmatic approach to prevent interdiffusion has so far been the choice of two multilayer materials with a low degree of intermixing, obviously a choice which is limited by the optical constants of such materials. Alternatively, the surface reactivity of the layers can be modified, for instance by H passivation of especially Si (Si:H). Due to the binding of H to dangling bonds of the Si surface, diffusion of a third material into the Si is suppressed.[5] However, an undesirable side effect is the formation of island like growth. This is in general described by the Young Dupré equation[6] applied for the Si/W case:

$$\gamma_{Si} = \gamma_{W/Si} + \gamma_W \cos\delta \qquad (49a)$$

where γ_{Si} and γ_W are the surface energies of the Si surface and the W surface, respectively, and $\gamma_{W/Si}$ is the Si/W interface energy and δ is the contact angle of the W surface with the W/Si layer interface. In case no island formation occurs, this formula is changed into:

$$\gamma_{Si} \leq \gamma_{W/Si} + \gamma_W \qquad (49b)$$

resulting from the fact that no contact angle can be defined. Since the hydrogen passivation will result in a higher surface energy, $\gamma_{W/Si}$ (more energy is needed to create a W-Si interface), while the Si surface energy, γ_{Si}, is reduced by the passivation. This may result in island formation or an increase of the contact angle. This effect has for example been observed in Si:H/Mo structures,[7] and becomes apparent on a macroscopic scale as a 'wetting' problem.

To overcome this issue, we here propose the application of a separate, atomically thin adhesion layer on the H-passivated Si layers. The adhesion layer is meant to decrease the interfacial energy between W and Si and to increase the Si surface energy, which will result in larger W islands, or even a closed W layer. Though some sacrificial intermixing will take place in this adhesion layer, its effect is expected to be limited to the thickness of the adhesion layer (which can be chosen appropriately).

In the particular case of Si:H, an additional improvement of the multilayer performance may be achieved due to the reduced density of the silicon layer, resulting in an increased optical contrast within the bi-layer system.[8,9] A first experimentally produced system consisted of a Si:H/Si/W structure which, in a comparison with Si/W structures, showed a

reduced degree of intermixing while compared with Si:H/W structures a reduced island formation is found. In addition, a higher x-ray reflectivity was found.

6.3 Experimental

We used e-beam evaporation in an ultra high vacuum system (base pressure 10^{-9} mbar) to deposit Si and W on Si (100) substrates. The process was controlled in real time by in situ reflectometry using carbon-K radiation[1] at a grazing angle of incidence of 35°. This resulted in a multilayer periodicity of 4.1 nm, for application in the soft x-ray range. A Kaufman ion source, mounted under a grazing angle of 35°, provided the H^+-ions. The minimal energy required to implant H^+ in the full top Si layer was calculated using the computer programme SRIM[10] resulting in a value of 10 eV. However, our Kaufman ion source required 500 eV to reach the needed dose[9] in a reasonable implantation time (1000 s). Due to the low mass of the H^+ ions no layer intermixing[11] at sub-surface interfaces is expected to occur, despite the relatively high ion-energy. This was verified by SRIM simulations. It is noted that for the purpose of reducing the intermixing between W and Si it would be sufficient to only passivate the dangling bonds at the Si surface, while for the increase in optical contrast due to the reduced density of Si the full Si layer should be implanted with hydrogen.

Planar bright field transmission electron microscopy (BF-TEM) was used to determine the lateral homogeneity of the growth of the W layer. These samples were produced by depositing the layers on crystalline NaCl substrates, in parallel to the standard Si (100) substrates. After deposition, the structures were isolated by dissolving the NaCl in water, and transferred to a copper grid. This way, a set of three TEM samples was deposited, each consisting of a 12.6 nm thick Si support layer followed by one period of Si/W (Figure 35a), one period of Si:H/W (b), or one period of Si:H/Si/W(c). Each deposited Si layer was smoothened by etching ~0.5 nm using 300 eV Kr^+ ions. Hydrogen was then

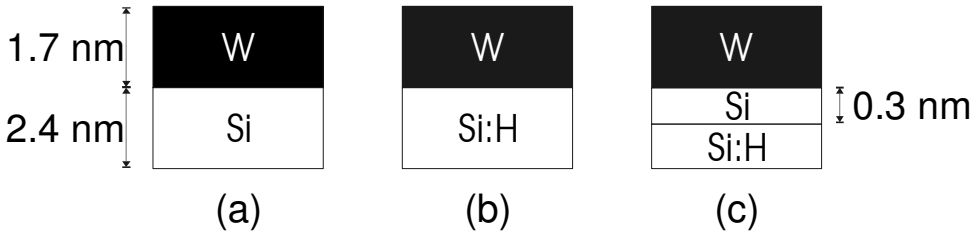

Figure 35 Visualisation of one period of the three different structures: Si/W (a) Si:H/W (b), and Si:H/Si/W (c).

implanted into the silicon layer, while the ~0.2 nm swelling of the Si was followed by the in-situ layer thickness monitor. The Si:H/Si/W structure was produced by additionally depositing an ~0.2 nm thin Si layer: the adhesion layer between the passivated Si:H and the next deposited W layer. The total thickness of all Si, Si:H and Si:H/Si layers were equal to 2.4 nm. The thickness of the W was chosen such that the complete period was equal to 4.1 nm, i.e. 1.7 nm of W. In order to avoid any risk of extra intermixing of the W on (hydrogenated) Si interfaces, no ion smoothening was applied at the W surface in this work.[12] Finally a Si layer of 4.1 nm was deposited to shield the W layer from atmospheric influences.

We additionally produced sets of 10-period multilayer systems to allow x-ray reflectivity measurements. These systems were fabricated using the same procedure. The total H^+ content after deposition of the multilayer structure was determined by elastic recoil detection (ERD) using 2 MeV He^+ ions which impinged on the sample under 15 degrees grazing incidence with the surface. The recoiled hydrogen particles were detected by a silicon detector at an angle of 35 degrees with the incoming beam. In front of the detector a 9 μm Mylar stopper foil was mounted to stop the scattered He ions.

6.4 Results

Figure 36 shows the planar TEM micrographs of the three types of samples. The W-on-Si layer (Figure 36a) shows a laterally homogeneous and closed layer. This is in contrast to the structure of the W layer deposited on the H-implanted Si (Figure 36b and c), which shows island formation. The average lateral dimensions of these islands were determined using a method described by Pilling,[13] which is based upon the determination of the average distance between edges of islands, and amounted less than or equal to 2.95 ± 0.03 nm (in the case of Si:H/W) and 3.62 ± 0.03 nm (Si:H/Si/W).

Table 3 shows the peak value of the in-situ reflectivity measured as a function of the period number, for respectively the Si/W, Si:H/W and Si:H/Si/W multilayer. A significant

structure	Reflectivity (R/R_0)
Si/W	41±4
Si:H/W	26±4
Si:H/Si/W	48±4

Table 3 Measured in-situ soft x-ray reflectivities of ten period structures relative to the initial reflectivity R_0 of the substrate.

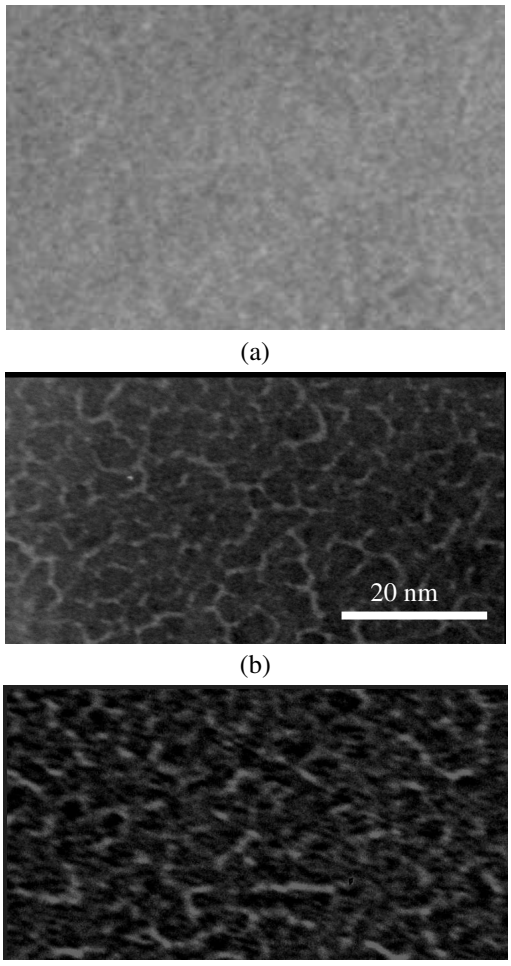

(a)

(b)

(c)

Figure 36 Planar TEM micrographs of a W layer on top of respectively Si (a), Si:H (b), and Si:H:Si (c). Visible is the difference between the W-on-Si (homogeneous and closed) and the two hydrogenated systems (voids in the W layer).

relative drop (-37±9%) in reflectivity is observed of the hydrogenated Si:H/W compared to the standard Si/W multilayer. The addition of the Si adhesion layer in the Si:H/Si/W more than compensates this loss and results in a 18±9% higher reflectivity relative to the standard multilayer. In a second set of samples these results were reproduced.

The total H content in the 10 period multilayer was equal to 2.6 x 10^{16} ± 5% atoms/cm^2 for the Si:H/W structure and 4 x 10^{16} ± 5% atoms/cm^2 for the Si:H/Si/W structure.

Assuming that all H is located in the treated Si layers, which had an initial density of 90% of the Si bulk density,[9] and assuming that no sputtering of Si occurred during H bombardment, we find a H fraction of 24 vol% and 34 vol% respectively. This corresponds to 0.26 H atom per Si atom and 0.41 H atom per Si atom respectively.

6.5 Discussion

The differences in reflectivity between the three types of structures can be ascribed to a combination of intermixing, optical contrast, and size of the effectively reflecting surfaces. Each of these effects can be estimated, allowing us to verify their global contributions. We may assume that due to the passivating effect of hydrogen, the W on Si:H interface is more abrupt than the W on Si interface. To a lesser extend, this will also be valid for the W on Si:H:Si interface, since here less than 0.2 nm of Si is 'available' for intermixing with W. The reduction of the, for W-on-Si typically 0.6 nm[14] thick, interface layer to ~0.3 nm would result in a relative increase of the reflectivity to ~40%, indicating an upper boundary in the reflectivity gain from this effect.
Based on the higher contrast between Si:H and W as compared to Si and W, using the determined densities of the H-implanted Si layer, an additional relative increase of ~40% of the reflectivity can be expected.
Both these factors, having a positive effect on the reflectivity, are counterbalanced by a third effect, namely the reduction of the effectively reflecting surface due to the island structure of the W layer (Figure 36). In a first order approximation we may assume that the visible, 0.5 nm wide boundaries of the islands do not contribute to the reflection process, as well as the width of half a W atom (~0.15 nm) at the edges of the islands. This results in effectively reflecting surfaces of only 53% in the case of Si:H/W, and 61% in the case of Si:H/Si/W, both as compared to 100% for the Si/W system.
Taking the above three factors into account, we find that their total effect on the reflectivity agrees reasonably well with the experimental reflectivity data, namely a relative reduction of the reflectivity by 25% (vs. a measured 37±9%) for the Si:H/W structure and a gain of 9% (vs. 18±9% measured) for the Si:H/Si/W structure, both as compared to the reflectivity of the Si/W structure.
Additional analysis of particularly the W structure on top of Si:H and Si:H:Si for instance using in-situ STM, would be required to determine the most optimal thickness of the Si adhesion layer. If for example the size of the islands can be increased to 4.5 nm, without any increase of intermixing of W and Si, the expected reflectivity of the structure would be twice the reflectivity of the Si/W structure. The use of these adhesion layers holds

promise for further improvement of film properties like layer roughness and degree of intermixing.

6.6 Conclusions

The use of H implantation into the Si layers of Si/W multilayer structures, previously suggested to increase the optical bi-layer contrast, has experimentally been shown to result in the formation of island-like W structures, and a reduced multilayer reflectivity as compared to standard Si/W multilayers. These effects are explained by a reduced interface interaction between Si:H and W resulting from the H passivation of the dangling Si bonds. However, the addition of an adhesion interlayer to the H-passivated Si layer, was found to lead to improved W layer growth resulting in larger grains with reduced roughness and, consequently, a higher x-ray reflectivity. The improved layer growth properties are qualitatively described by modified surface and interfacial energies at the interfaces, and quantitatively explained by a combination of changed intermixing, optical contrast, and geometry of the reflecting surfaces.

6.7 Acknowledgments

The authors acknowledge H. Zeijlemaker for the technical assistance, Wim Arnoldbik for performing the ERD measurements, John de Geus for TEM measurements, and Eric Louis for helpful discussions. This work is carried out as part of the research programme of the Stichting voor Fundamenteel Onderzoek der Materie (FOM) with financial support from the Nederlandse Organisatie voor Wetenschappelijk Onderzoek (NWO).

6.8 References

[1] E. Spiller, (SPIE (Society of Photo-optical Instrumentation Engineers), 1994).

[2] This thesis: chapter 2, M.J.H. Kessels, J. Verhoeven, and F. Bijkerk, to be published.

[3] This thesis: chapter 3, M.J.H. Kessels, F.D. Tichelaar, J. Verhoeven, and F. Bijkerk, submitted.

[4] S. Bajt, J.B. Alameda, T.W. Barbee, W.M. Clift, J.A. Folta, B. Kaufmann, and E.A. Spiller, Opt. Eng. **41** (8), 1797 (2002).

[5] G. Palasantzas, B. Ilge, J. de Nijs, and L.J. Geerligs, Surface Science **412-413**, 509 (1998).

[6] M. Zinke-Allmang, Thin Solid Films **346** (1-2), 1 (1999).
[7] M. Lohmann, F. Klabunde, J. Blasing, P. Veit, and T. Drusedau, Thin Solid Films **342** (1-2), 127 (1999).
[8] R. Schlatmann, A. Keppel, Y. Xue, J. Verhoeven, and M.J. van der Wiel, Appl. Phys. Lett. **63** (24), 3297 (1993).
[9] R. Schlatmann, A. Keppel, Y. Xue, J. Verhoeven, C.H.M. Maree, and F. Habraken, J. Appl. Phys. **80** (4), 2121 (1996).
[10] J.F. Ziegler, SRIM the stopping and range of ions in matter (Annapolis, 2000).
[11] This thesis: chapter 5, M.J.H. Kessels, J. Verhoeven, A.E. Yakshin, F.D. Tichelaar, and F. Bijkerk, Nucl. Instrum. Meth. B **222** (3-4), 484 (2004).
[12] This thesis: chapter 3, M.J.H. Kessels, F.D. Tichelaar, J. Verhoeven, and F. Bijkerk, Journal of Applied Physics, submitted (2004).
[13] J. Pilling, (http://callisto.my.mtu.edu/my3200/lab1/grainsize.html).
[14] This thesis: chapter 4, M.J.H. Kessels, J. Verhoeven, F.D. Tichelaar, and F. Bijkerk, to be published (2004).

7 Summary

This thesis describes the design, production, and characterization of multilayer mirrors intended as wavelength dispersive elements for the soft x-ray range. The central theme is the analysis and control of the different processes occurring at the materials interfaces between the layers. These interfaces largely determine the multilayer optical characteristics and form a continuous challenge to improve the multilayer performance, i.e. its optical reflectivity and wavelength selectivity. Both properties are of relevance for the main application motivating this particular work, namely X-Ray Fluorescence spectroscopy (XRF). XRF is an elemental analysis technique for which multilayer dispersive elements are employed. The results collected in this thesis, however, also deal with more general thin film phenomena of relevance for other thin single and multilayer systems in microelectronics and elsewhere.

The ability to freely design and synthesize multilayer mirrors has in the past led to experimental and theoretical approaches to increase the multilayer wavelength selectivity. This was done by modifying the ideal, block-shape, density profile of a multilayer of two pure materials with perfectly sharp interfaces into a profile with a certain gradient within the materials density. However, so far, no general theory has existed that includes the effect on the reflectivity of such modifications. This thesis includes such a theoretical proof, namely stating that the ideal, classical design in all cases leads to the highest reflectivity for any given selectivity. For this purpose, a Fourier theory about reflection in multilayer optics was used, taking into account the effect of absorption on the penetration depth of the radiation. However, the use of graded density multilayer systems does have the advantage that a certain target selectivity can be reached at slightly higher metal fractions in the bi-layer, which is favorable for the practical fabrication.

Obviously, in the experimental programme of fabricating these and other density profiles, it is imperative to avail oneself of a clear method to determine the actual profiles created in the samples. Although numerous analysis methods do exist, they either alter the structure prior to the analysis or require extensive knowledge of the structure beforehand. In this work a new technique has been developed, which allows extracting quantitative information on materials densities from cross-section transmission electron microscopy (TEM) images. Using TEM it was already possible to obtain a qualitative in-depth density profile of the structure. By combining this technique with x-ray reflectometry, this intensity profile can now be converted into a calibrated density profile. The technique is demonstrated for W/Si and Mo/Si multilayers with sharp interfaces as well as multilayers of which the interfaces were deliberately intermixed. The in-depth density profile, the layer thickness, the layer roughness and even the stoichiometry for each individual layer in the structure could accurately be determined.

The use of these and other analysis methods have revealed clearly the effects of different forms of ion treatment, commonly applied to improve the reflectivity of multilayer mirrors. Dependencies of film properties were investigated for respectively low and high energies of the ions impacting during or after deposition of W layers in W/Si multilayer mirrors. Analysis revealed that the addition of energy to the W layer resulted in a smoother surface of the W layer, and thus a sharper interface with the next deposited Si layer. This positive effect was (partly) counter balanced by ion-induced intermixing of the W-on-Si interlayer below, due to the penetration of ions through the thin (2 nm) top W layer. For higher ion energies it was observed that the intermixing at the latter interface increased, ultimately leading to a complete intermixing of W into the Si layer. Combining the effects at the Si-on-W and the W-on-Si interface, an optimal energy for the ion treatment was determined having a net positive effect on the reflectivity. Chemical affinity between Si and W was identified as a main reason for the intermixing.

The studies on this and other types of layer intermixing have led to the formulation of a method to control interface intermixing phenomena. It is based on H-passivation of the Si layer and the subsequent deposition of an atomically thin Si layer acting as an adhesion layer. Upon W-overcoat, the latter is converted into silicide of which the thickness is limited due to the finite amount of unpassivated Si. Using planar TEM analysis it was confirmed that deposited W chemically hardly interacted with the Si:H:Si layer underneath. The Si:H/Si/W multilayer mirror showed an 18 rel.% higher reflectivity than the conventional Si/W mirror.

8 Samenvatting

Dit proefschrift beschrijft het ontwerp, de productie en de analyse van multilayer spiegels die toegepast worden als dispersieve elementen voor zachte röntgenstraling (0.1 tot 10 nm). Centraal staat de analyse en beïnvloeding van die processen welke plaatsvinden in de grenslagen tussen de verschillende materiaallagen in de spiegels. Deze grenslagen bepalen in belangrijke mate de optische eigenschappen van multilayer spiegels. Het is daarom een uitdaging om de fysisch-chemische eigenschappen van deze grenslagen te beheersen zodat de reflectie kan worden verbeterd, of de gewenste golflengteselectiviteit kan worden gerealiseerd. Deze twee eigenschappen zijn van groot belang voor toepassing van de multilayer spiegels in röntgenfluorescentieanalyse. In deze techniek wordt het dispersieve karakter van multilayer spiegels gebruikt om element-specifieke fluorescentiestraling te analyseren. De resultaten samengevat in dit proefschrift zijn echter ook toepasbaar op enkelvoudige dunne lagen en multilayer sytemen in bijvoorbeeld de micro-electronica.

In het verleden is veelvuldig geprobeerd om zowel experimenteel als theoretisch de flexibiliteit in het ontwerp van multilayer systemen te benutten om de golflengteselectiviteit te verhogen. Hierbij werden de in theorie scherpe grenslagen vervangen door grenslagen met een eindige dichtheidsgradient. Hoewel dit incidenteel inderdaad resulteerde in structuren met een hogere selectiviteit, ontbrak tot dusver een algemeen bewijs dat dit ook daadwerkelijk de meest optimale structuur was. Dit proefschrift bevat zo'n bewijs en het blijkt dat structuren met een dichtheidsgradient aan de grenslaag niet ideaal zijn, en dat een structuur met scherpe grenslagen altijd resulteert in een hogere reflectiviteit voor elke gewenste selectiviteit. De argumentatie is gebaseerd op een toepassing van de Fourier theorie op de reflectie van multilayer systemen gecombineerd met de eindige penetratiediepte van de straling. Hoewel scherpe grenslagen in theorie dus optimaal zijn, kan het vanuit het oogpunt van de fabricage van deze dunne film systemen soms gunstiger zijn om toch een materiaaldichtheidsgradient toe te staan.

Hierdoor kan bijvoorbeeld met een hogere metaalfractie toch een hoge selectiviteit bereikt worden.

Voor een juiste analyse van de geproduceerde multilayer structuren is het onontbeerlijk om over een methode te beschikken waarmee eenduidig de structuur kan worden bepaald. Alle bestaande methodes hebben het nadeel dat de structuur veranderd wordt voor of tijdens de meting, of er dient gebruik gemaakt te worden van veel a priori aannames. In dit proefschrift demonstreren wij een methode om kwantitatieve informatie uit een elektronenmicroscopie-opname van een dwarsdoorsnede van de structuur te halen. Met TEM was het reeds mogelijk om kwalitatieve diepte-afhankelijke intensiteitprofielen te verkrijgen. Door deze techniek te combineren met röntgenreflectometrie kunnen deze profielen omgerekend worden in gekalibreerde dichtheidsprofielen. In dit proefschrift geven we een demonstratie van deze methode op W/Si en Mo/Si multilayer spiegels waarbij de raakvlakken ofwel scherp zijn, ofwel opzettelijk diffuus zijn gemaakt. Zowel de diepteafhankelijke dichtheid, de laagdiktes, de ruwheden van de raakvlakken en zelfs de stoichiometrie voor elke individuele laag kon op deze manier worden bepaald.

Door gebruik te maken van deze en andere analysetechnieken is het effect van verschillende ionenbehandelingen, zoals veelvuldig gebruikt voor het verbeteren van de laageigenschappen van dunne films, duidelijk geworden. Zo is onderzocht wat de invloed op de uiteindelijke structuur is van ionenbombardement tijdens of na de depositie van een wolfraam laag als functie van de ionenenergie. Uit deze analyse bleek dat de toevoeging van energie aan de W laag resulteerde in een vlakker oppervlak van deze laag, met als resultaat een meer stapvormige overgang tussen de W laag en de daarop gedeponeerde Si laag. Echter, dit positieve effect werd gedeeltelijk tenietgedaan door een verhoogde vermenging in de grenslaag tussen W en het onderliggende Si, veroorzaakt door de indringdiepte van de ionen in de dunne (2 nm) W laag. Verhoging van de ionen-energie resulteerde in een sterkere vermenging, met als uiteindelijk resultaat een volledige vermenging van het W met het onderliggende Si. Door beide effecten op de W-op-Si en Si-op-W grenslagen te combineren, kon een optimale ionen-energie bepaald worden, zodanig dat er netto een positief effect was op de reflectiviteit van de structuur. Het vermengen van het W met het onderliggende Si kon verklaard worden op basis van de chemische affiniteit tussen W en Si.

Deze en andere analyses van vermenging van de lagen hebben geleid tot een nieuwe methode om deze vermenging te verminderen. Deze methode is gebaseerd op H-passivatie van de Si laag, waarbij vervolgens een atomair dunne laag van Si als adhesielaag wordt

aangebracht. Tijdens W depostitie wordt dan een W-silicide laag gevormd. Vanwege de beperkte hoeveelheid niet gepassiveerd Si in de laag is deze silicide in dikte beperkt. Met behulp van loodrecht op het oppervlak gemeten TEM kon aangetoond worden dat het gedeponeerde W vrijwel geen interactie had met de onderliggende Si:H:Si laag. De Si:H/Si/W multilayer spiegel had daardoor een 18% hogere reflectiviteit dan de standaard Si/W spiegel.

9 Dankwoord

Na 189 deposities gedaan te hebben (waarvan 1 op Rijnhuizen) met dank aan Hans en de technici van Rijnhuizen, 134 759 letters ingetikt te hebben (zonder de geschrapte teksten mee te tellen, waarvoor dank verschuldigd is aan Jan, Fred, Niek, Aart, Robbert, Andrey en Eric), drie defecte harddisks (waarvan twee in één week, origineel en backup dus weg… met dank aan Murphy), drie laptops (wederom met dank aan Murphy), twee turbopompen, ontelbare proefballonnetjes van Jan afgeschoten (de goede ideeën staan nu dus in dit proefschrift), 480 RVS bouten los, en daarna weer vast gedraaid, vooral als er weer eens iemand 'hoppaa' schreeuwde (ik zal geen namen noemen), een voorbeeld spiegel van Walter, 216 363 simulaties, uitgevoerd op de computers van mijn collega's, honderden TEM foto's, voor een groot deel gemaakt door Frans, drie opstellingen geautomatiseerd samen met Guus, Gideon en Sjoerd, 5 SIMS metingen door Katrien, een SEM meting en een aantal EDX metingen door Chris, 2 ERD metingen door Wim, een niet nader te noemen aantal keren mijn frustratie bij Eric kunnen uiten, many discussions with Andrey, especially about what should be considered as a good fit, many attempts to get more information out of reflectometry measurements together with Igor, vijf druppels wonderolie van Wim als ik weer eens een moertje te vast had gedraaid, het gasregelkastje van Michel, een database, waarbij de gebruikersinterface is gemaakt door Dave, Rudy, Martijn, Santi, en vooral Matthijs, vele kilometers zwemmen, waarbij ik gesteund werd door vele oproepen van zwemmers@rijnh.nl, het vele malen mee mogen rijden in de bus (tegenwoordig beter bekend onder de naam 'groene kliko') van André, sloten koffie gedronken en gezellig gediscussieerd te hebben met mijn collega's, vele aanmoedigende woorden van Debby en mijn ouders, en, last but not least, goedkeuring te hebben ontvangen voor mijn proefschrift (het verlossende woord werd uitgesproken door Klaus), kan ik eindelijk zeggen:
Bedankt allemaal,

't is vaerdig.

10 Curriculum vitae

Marc Kessels werd geboren op 22 april 1977 te Roermond. Vanaf 1989 studeerde hij aan het bisschoppelijk college Echt. In 1995 behaalde hij met lof het VWO diploma in acht vakken. Aansluitend studeerde hij technische natuurkunde aan de Technische Universiteit Eindhoven. Het afstudeerwerk verrichtte hij in de groep “laserplasma’s en XUV optica” van dr. F. Bijkerk aan het FOM Instituut voor Plasmafysica Rijnhuizen, onder supervisie van prof. dr. M.J. van der Wiel van de TU Eindhoven. De titel van dit afstudeerwerk is “Controlling the lateral distribution of thicknesses during deposition of thin films with sub nanometer precision”. Het doctoraalexamen aan de Technische Universiteit Eindhoven werd afgelegd op 27 juni 2001. Op 1 oktober 2000 startte hij als promovendus met het promotieonderzoek dat resulteerde in dit proefschrift. Dit onderzoek werd zowel op het FOM Instituut voor Atoom- en Molecuulfysica (AMOLF) uitgevoerd als op het FOM Instituut voor Plasmafysica Rijnhuizen onder dagelijkse begeleiding van ir. J. Verhoeven en supervisie van Dr. F. Bijkerk.